This is the peer-reviewed, final accepted version for American Mineralogist, published by the Mineralogical Society of America.
The published version is subject to change. Cite as Authors (Year) Title. American Mineralogist, in press.
DOI: https://doi.org/10.2138/am-2021-7612. http://www.minsocam.org/


revision 1

# Ultra-reduced phases in ophiolites cannot come from Earth's mantle

Chris Ballhaus[1]*, Hassan M. Helmy[1], Rául O.C. Fonseca[2], Richard Wirth[3], Anja Schreiber[3], Niels Jöns[2]

[1]Geoscience Institute, University of Bonn, Germany

[2]Institute for Geology, Mineralogy and Geophysics, Ruhr-University of Bochum, Germany

[3]Helmholtz Centre Potsdam, GFZ German Research Centre for Geosciences, Potsdam, Germany

* corresponding author (email: ballhaus@uni-bonn.de)

Key words: ultra-reduced minerals, moissanite, ultra-reduced mantle, ophiolites, oxidation state

## ABSTRACT

A number of recent papers have purported to find ultra-reduced minerals - as natural examples - within ophiolitic mantle sections, including SiC moissanite, Fe-Si alloys, various metal carbides, nitrides, and borides. All those phases were interpreted to be mantle derived. The phases are recovered from mineral concentrates and are assigned to the deep mantle because microdiamonds and other ultra-high pressure (UHP) minerals are also found. Based on these findings it is claimed that the mantle rocks of ophiolite complexes are rooted in the Transition Zone (TZ) or even in the Lower Mantle, at redox states so reduced that phases like SiC moissanite are stable.

We challenge this view. We report high temperature experiments carried out to define the conditions under which SiC can be stable in Earth's mantle. Mineral separates from a fertile lherzolite xenolith of the Eifel and chromite from the LG-1 seam of the Bushveld complex were reacted with SiC at 1600K and 0.7 GPa. At high temperature a redox gradient is quickly established between the silicate/oxide assemblage and SiC, of ~ 12 log-bar units in $fO_2$.

Reactions taking place in this redox gradient allow to derive a model composition of an ultra-reduced mantle by extrapolating phase compositions to 8 log units below the iron-wüstite equlibrium (IW-8) where SiC should be stable. At IW-8 silicate and oxide phases would be pure MgO endmembers. Mantle lithologies at IW-8 would be Fe° metal saturated, would be significantly enriched in $SiO_2$, and all transition elements with the slightest siderophile affinities would be dissolved in a metal phase. Except for the redox-insensitive $MgAl_2O_4$ endmember, spinel would be unstable. Relative to an oxidized mantle at the fayalite-magnetite-quartz (FMQ) buffer, an ultra-reduced mantle would be enriched in enstatite by factor 1.5 since the reduction of the fayalite and ferrosilite components releases $SiO_2$. That mantle composition is unlike any natural mantle lithology ever reported in the literature. Phases as reduced as SiC or Fe-Si alloys are unstable in an FeO bearing hot convecting mantle. Based on our results we advise against questioning existing models of ophiolite genesis because of accessory diamonds and ultra-reduced phases of doubtful origin.

## INTRODUCTION

Until recently it was thought that ophiolites form by spreading of oceanic lithosphere at shallow (~ 50 km) depth (Nicholas, 1999; Pearce and Robinson,

2010; Dilek and Furnes, 2014), most commonly above intra-oceanic subduction zones (Miyashiro, 1973; Robertson 2002). The discovery of UHP minerals in ophiolites worldwide (Robinson et al., 2004; Yang et al. 2015) challenges that view. New models now propose that the mantle lithologies of ophiolites are rooted in the transition zone (TZ) or even in the lower mantle (Griffin et al., 2016a). Some authors even claim that the characteristic ores of supra-subduction zone ophiolites - podiform chromite mineralisations - are enriched at TZ pressure when chromite is in the post-spinel stability field (Xiong et al., 2015).

But how credible are those models? Do microdiamonds in ophiolite lithologies justify rewriting the entire history of ophiolite genesis? The problem is that ophiolitic diamonds are found almost exclusively in heavy mineral concentrates of harzburgite and chromitite bulk samples up to 1000 kilos in size (Robinson et al., 2004; Xu et al., 2015; Yang et al., 2015). The risk of contamination during sample processing is high. Except for three dubioius examples (Yang et al., 2007; 2015; Das et al., 2017) - two of the in-situ diamonds occur in carbon glass - no cases are reported where diamonds were found intergrown with mantle minerals.

In addition to diamonds, the mineral separates return ultra-reduced minerals including SiC, Fe-Si alloys, metal nitrides, carbides, and borides (Fig. 1). These phases also pose a problem. Ophiolites are lithologies that crystallize at oxygen fugacities ($fO_2$) around FMQ. Silicon carbide and Fe-Si alloys, by contrast, afford $fO_2$ conditions of ~ IW-8 (Barin, 1995). At this relative $fO_2$ mantle silicates should be FeO-free, should coexist with (Fe,Ni) metal, and $Cr_2O_3$ in chromite would be reduced to metallic Cr (Schmidt et al., 2014; Golubkova et al., 2016). No such signatures have ever been reported from mantle lithologies.

The diamonds are not the topic of this paper even though their relation to ophiolite lithologies is far from being understood: many "ophiolitic" diamonds carry Mn-Ni-

Co metal inclusions (Yang et al., 2014; 2015; Griffin et al., 2016a), a composition that is used in China as solvent-catalyst to flux industrial diamond synthesis (Sund and Tai, 1997; Zhou et al. 2009; Tan, 2014); those "ophiolitic" diamonds that were analysed for their nitrogen aggregation states are 1B diamonds (Howell et al., 2015; Xu et al., 2017), not exactly a signature consistent with long residence times in the deep mantle; and where "diamondiferous" ultramafic rocks of ophiolite sequences are associated with gabbroic cumulates the latter lack evidence for an UHP overprint (Ballhaus et al., 2018a). We focus here on the ultra-reduced phases (Fig. 1). We report reaction experiments in redox gradients in which mantle silicates and chromite are reacted with SiC. The experiments are intended to clarify (1) if an SiC grain can be stable at ambient mantle temperature and redox state, (2) for how long it would survive the uplift from deeper mantle levels, and (3) what textural and compositional changes a mantle would undergo when it is are exposed to ultra-reduced conditions. The last point allows to identify compositional fingerprints of ultra-reduction, should such fingerprints ever be found in Earth mantle lithologies.

## METHODS

Starting materials for the redox experiments were 65 wt.% lherzolitic materal from a fertile xenolith from Dreiser Weiher (Eifel), 25 wt.% metallurgical-grade chromite from the LG-1 layer of the Bushveld Complex, and ~ 10 wt.% industrial hexagonal SiC. Silicate and oxide phases had grain sizes around 100 µm. Silicon carbide was added in two grain sizes; ~ 1 to 10 µm for the run cr-6 (2 hrs), and as angular grains 100 ± 50 µm in size for the runs cr-8 (4 hrs) and cr-9 (30 min). Aliquots of the materials were loaded in 4 mm outer diameter graphite capsules, then reacted in a piston-cylinder press at 1600K and 0.7 GPa. The pressure

transmitting media were talc-pyrex sleeves. The heating elements were 5 mm inner diameter graphite rods machined from high resistance graphite. To avoid short circuiting, the graphite capsules were shielded from the heaters by 0.5 mm thick boron nitride sleeves. Temperature was controlled with W-Re thermocouples to within ± 20K. Quenching occurred by turning off power supply.

At the beginning of a run when the target temperature of 1600K was approached, a redox gradient of ~ 12 log-bar units developed inside the capsules between the mantle material, chromite, and SiC (Fig. 2). The mantle minerals plus chromite define an $fO_2$ at FMQ (Ballhaus et al., 1991) while SiC imposes at 1600K an upper $fO_2$ limit at ca. IW-8 (Barin, 1995). Thermodynamic equilibrium was not reached but this was not intended. Tje aim instead was to document reactions along a redox gradient, in order to quantify if and for how long ultra-reduced phases like SiC may survive in oxidized (± FMQ) mantle.

Phases were analysed and imaged with a Cameca SX FIVE FE microprobe at the Ruhr University Bochum using natural and synthetic materials as standards (Table 1). Selected textures were imaged at high high resolution with a Zeiss Gemini Sigma 300 VP FE Scanning Electron Microscope (SEM) at the University of Cologne. Many reaction products were too fine-grained to be resolved and quantified by electron probe micro-analysis (EPMA) or SEM. Therefore, four Focussed Ion Beam (FIB) foils were cut (Wirth 2009) from one polished section of the run cr-6 and investigated for reaction textures with a FEI F20 X-Twin Transmission Electron Microscope (TEM) at the GFZ in Potsdam.

## RESULTS

This is the peer-reviewed, final accepted version for American Mineralogist, published by the Mineralogical Society of America.
The published version is subject to change. Cite as Authors (Year) Title. American Mineralogist, in press.
DOI: https://doi.org/10.2138/am-2021-7612. http://www.minsocam.org/


In Figure 3 we summarise backscattered electron (BSE) images and element distributions of relevant phases and textures. Phases identified are two (relict and product) generations of olivine and orthopyroxene, one generation of clinopyroxene, and three generations of spinel. Minor phases are (Fe,Ni), (Fe,Cr), and Fe-Cr-Si metal alloys, relict SiC, metallic Si, and silicate glass pools. Figure 4 documents element distributions to illustrate qualitative compositional changes with progressive reduction. Many reactions are only discernible on the nanoscale, and for that reason we display in Figure 5 TEM images that document phases not resolvable by EPMA. The positions of the FIB foils are marked on Figure 3A and G.

*Silicates*

Olivine of the starting material (analysis 1) reacted with SiC either by forming localised reaction rims (Fig. 3A) or by whole-sale reduction (Fig. 3B to D). The reduction reaction is

$$(Fe,Ni)_2SiO_4 \text{ (in olivine)} + SiC = 2(Fe,Ni)^\circ \text{ (metal)} + 2SiO_2 + C \text{ (graphite capsule)} \quad (1)$$

Product phases are a second generation of olivine, Ni-free within EPMA detection limit (~ 200 ppm) but significantly more magnesian than olivine of the starting mix (analyses 4 to 6). On the nanoscale, product olivine is peppered with an α-(Fe,Ni) metal phase (Fig. 5A). The most forsteritic, post-reduction olivine composition analysed was $Fo_{98}$ but given the sizes and abundances of nanoscale α-(Fe,Ni) inclusions there is no guarantee that $Fo_{98}$ indeed is the most magnesian composition.

Relative to the primary starting olivine, reduced olivines are enriched in Cr to up to 3.6 in Cr oxide (analyses 4 to 6). This concentration seems excessive but several analyses on different grains confirmed this to be the case. Normally, mantle olivine at around FMQ carries Cr as a trace constituent (analysis 1) and Cr is trivalent (Li et al., 1995). In highly reduced Moon basalts (Haggerty, 1978) olivine phenocrysts do contain Cr in the percentage range, and Cr is at least in part divalent (Schreiber, 1979; Sutton et al., 1993; Li et al., 1995) but not as Cr enriched as here. We have calculated here Cr in the reaction olivines tentatively as a CrO component (Table 1) to satisfy the cation-oxygen (3:4) ratio of olivine (Table 1).

Reaction (1) sets free $SiO_2$ both by reduction of fayalite to metallic Fe and by the oxidation of SiC to $SiO_2$. We expected that inside the reduction rims (Fig. 3A) orthopyroxene rather than olivine would be stable but that phase was not identified in the rims. We do note both relict and product orthopyroxene outside the reduction rims in the groundmass (analyses 2 and 7), the latter usually as microcrysts in glass (former melt) pools. Reduced orthopyroxene is nearly as magnesian as reduced olivine ($En_{96}$) and quite enriched in Cr. To satisfy cation-oxygen stoichiometry constraints we calculated Cr as CrO (analysis 7).

*Oxides*

Chromite also reacted with SiC (Fig. 3E to G). It was surprising to note how quickly and easily a phase as refractory as LG-1 chromite disintegrated upon exposure to SiC (IW-8). The original Bushveld chromite (analysis 3 in Table 1) decomposed to inclusion-rich grain aggregates with several generations of spinel (analyses 8 to 11) highly variable in their Cr/Al and Mg/(Mg+Fe) atomic ratios. In BSE images (Fig. 3E to G) and in the element maps (Fig. 4) secondary spinels are

easily recognised by their lower atomic number contrasts and by ultra-fine < 1 μm wide (Fe,Cr)° metal veinlets. On the nanoscale, reduced spinels are peppered with euhedral (Fe,Cr) metal inclusions up to 200 nm in size (Fig. 5B,C). One FIB foil through a secondary spinel returned, in addtition, ferroan periclase inclusions. We assume that this phase is an excess product left over after FeO, $Fe_2O_3$, and $Cr_2O_3$ were reduced to metal components.

We identify three generations of spinel (Fig. 6): relicts of LG-1 chromite (in black); a compositional array (in red) trending with progressive reduction toward slightly elevated Cr# and much increased Mg# and corresponding to the low atomic contrast spinel rims around LG-1 relicts visible in Fig. 3E, F, and H; and a spinel generation markedly enriched in Al component (in red). This generation is noted near silicate melt (now glass) pools (Fig. 3G) and seems to have exchanged Cr and Al by reaction with melt.

We note that some secondary spinels have slight cation excesses when their stoichiometries are calculated to 4 oxygens. Normally, one would then calculate some FeO as magnetite component, however, for spinels that carry (Fe,Cr) metal inclusions this would seem unintuitive. The bright field image in Fig. 5D indicates that reduced spinels are defect-rich, hence may not be stoichiometric. Chromium in spinel was calculated throughout as an $MCr_2O_4$ ($Cr^{3+}$) component (Table 1) even though at 1600K and the relative $fO_2$ (see below) much of the bulk Cr may have been divalent (Li et al., 1995; Berry and O'Neill 2004). Stubican and Greskovich (1975) presented experiments to show that owing to its high octahedral field stabilisation energy the $Cr^{3+}$ cation is strongly fractionated by spinel but $Cr^{2+}$ in spinel does occur.

*Reduced phases*

In the 2-hour run cr-6 SiC does not seem to have survived. Silicon carbide was added to this run rather fine-grained to promote rapid reduction. In the two other runs with 100±50 µm grain sizes SiC did survive (Fig. 3I) although local oxidation is evident. After only 30 min at 1600K relict SiC grains are surrounded by up to 5 µm wide reaction rims. The rims (Fig. 3J) carry nano-sized $SiO_2$ phases (? tridymite), are highly porous, and are reminiscent of solution-precipitation textures documented by Putnis (2002). Additional ultra-reduced phases include rare metallic Si, likely to be an impurity in the industrial-grade SiC starting material, plus heterogeneous (Fe,Ni,Cr,Si) metal phases: Ni enriched near olivine, Cr enriched when the metal is intergrown with spinel, and Si enriched near relict SiC grains. Larger metals can be exsolved (Fig. 3K), notably those enriched in Si. One single grain of metallic Cr was found (bright spot in Fig. 3K) but that grain must be metastable. In a bulk system with excess molar FeO over $Cr_2O_3$ and metallic Fe, metallic Cr should dissolve in the Fe metal phase.

*Oxygen fugacity prior to quenching*

The coexistence of olivine ($Fo_{98}$) with (Fe,Ni) metal permits to approximate the relative $fO_2$ prior to quenching using the equilibrium $Fe_2SiO_4 = 2Fe + SiO_2 + O_2$ and $\log fO_2 = \Delta G_{r,T} / (2.3 * R * T) + \log a_{Fa}^{ol} - 2 \log a_{Fe}^{metal} - \log a_{SiO2}^{glass}$. Olivine solid solutions are symmetric with a Margules parameter around 3 kJ $mol^{-1}$ (Wiser and Wood, 1991; O'Neill et al., 2003) but given the low fayalite content ($X_{Fa}^{ol} = 0.02$) and a run temperature of 1600K we suggest that $a_{Fa}^{olivine} = X_{Fa}^{2}$ is considered sufficiently precise. For iron in the (Fe,Ni) metal phase we ignore the Ni content (around 1 wt.% with local variations) and set $a_{Fe}^{metal}$ at unity. The $SiO_2$ activity is

approximated from the average mole fraction of $SiO_2$ in orthopyroxene saturated silicate glasses to 0.4. It follows that the $fO_2$ gradient, initially ~ 12 log-bar units, must have converged with run time to around IW-3 to IW-3.5 (Fig. 2). No fundamental differences are noted among the runs or with run time.

## DISCUSSION

It is clear from the results that at best local (grain-scale) redox equilibrium was achieved. We found relict and product olivine and orthopyroxene. We identified a range of spinel compositions that would have been homogenized to one phase had the runs not been quenched before global (capsule-scale) equilibrium was reached. The Cr, Ni, and Si concentrations in Fe metal are variable and controlled by local-scale environments. We identified three Cr oxidation states if the allocations of Cr to olivine (divalent), spinel (trivalent), and metal phases (zero) in Table 1 are correct. Note though that multiple Cr oxidation states are not necessarily indicative of disequilibrium (cf. Rohrbach et al., 2007). At IW-3 and 1600K three Cr oxidation states may have coexisted even though $Cr^{2+}$ should have been by far the prevalent species (Berry and O'Neill, 2004). Each Cr-bearing phase would then fractionate the Cr species that is most easily accommodated in its lattice.

### *The mantle at IW-8*

We may extrapolate the redox reactions to IW-8 and derive a model mantle composition that would be stable with SiC. Silicates would be reduced to their MgO endmembers, and their FeO and NiO components would be precipitated as (Fe,Ni) metal phase (cf. O'Neill and Wall, 1987). Reduction of fayalite and ferrosilite liberates $SiO_2$ (eqn. 1), hence modal orthopyroxene would increase. That

increase would not be insignificant: a harzburgite at FMQ with 80% $Fo_{92}$ and 20% $En_{92}$ reduced to IW-8 would liberate by fayalite and ferrosilite reduction 0.8 * 8 plus 2 * 0.2 * 8 moles of $SiO_2$ respectively, in total 9.6 moles $SiO_2$. A harzburgite in equilibrium with SiC would then be composed of ca. 70% forsterite and 30% enstatite plus a few percent metallic (Fe,Ni,Cr) alloys, compared to 80:20 (ol:opx) in a metal free harzburgite at FMQ.

At IW-8, spinel would have a small stability field. We do note that with progressive reduction Cr is enriched in spinel (cf. blue array in Fig. 6), however, our experiments were greatly enriched in chromite and no capsule-scale redox equilibrium was reached. In a reduced natural harzburgite at SiC the Cr, Ni, and Fe components would be reduced to (Fe,Cr) metal, and all transition elements with the slightest siderophile affinity would be dissolved in the Fe metal phase. The only spinel composition insensitive to reduction is $MgAl_2O_4$ but that endmember has a small stability field (Klemme and O'Neill, 2000). Above ca. 2 GPa, an ultra-reduced mantle composition would probably be garnet $(Mg,Ca)_3Al_2Si_3O_{12}$ saturated.

We do find mantle lithologies in Archaean cratonic lithosphere with vaguely similar signatures (Kelemen et al., 1992) but they are not metal saturated. Perhaps they were in the distant past?

*Ultra-reduced minerals - stable in upper mantle lithologies?*

Ultra-reduced phases like SiC or Fe-Si alloys or Ti carbides in ophiolites are highly unstable in Earth's mantle. Silicon carbide becomes oxidised quickly by reducing the FeO, NiO, and $Cr_2O_3$ components of mantle minerals to (Fe,Ni,Cr)° metal and divalent Cr. Reaction rates at 1600K (ambient asthenospheric temperature) are

rather fast, given that after only 30 min at 1600K SiC fragments are rimmed by up to 5 μm wide $SiO_2$ reaction rims (Fig. 3J). It is speculative to connect experimental reaction rates with mantle uplift rates, but we infer that convecting upper mantle at 400 km depths (cf. Xiong et al., 2015) would have to be exhumed within months to years to retain SiC grains 100 μm in size, much faster than uplift rates brought into discussion by Griffin et al. (2016a). Pressure has no significant effect. Even though our experiments were carried out at relatively low pressure (0.7 GPa) the $fO_2$ gradient of 12 log units (Fig. 2) can be safely extrapolated to the deeper mantle (Ulmer et al., 1998; Golubkova et al., 2016). Single oxygen buffers do have pressure terms but when the differences between two solid-state buffers are computed individual pressure effects largely cancel out.

*Ultra-reduced phases - textural and chemical considerations*

The ultra-reduced phases are unstable also on textural grounds. We illustrate this fact with characteristic textures illustrated in Figure 1.

Intra-grain exsolutions (Fig. 1A), symplectitic textures (Fig. 1B,C), and skeletal crystal morphologies (Fig. 1D-F) have rather unfavourable surface to volume ratios, and texturally they are highly unstable. Skeletal crystals typically grow in large temperature and/or chemical potential gradients when the rate of diffusion is slow relative to the cooling rate (Bryan, 1972; Donaldson, 1976). Such conditions are hard to reconcile for the asthenosphere. In a hot convecting mantle regime all those textures would recrystallise spontaneously to equant grains, in an effort to minimise their surface energies. They would not form in hot asthenosphere with no local (grain-scale) gradients, and even if they did form by some miraculous process

they would have no chance to survive uplift to Earth's surface for any length of time.

A rather critical case are the SiC grains in Figure 1G, one of the finds termed *"in-situ"* because SiC is enclosed by chromite. Liang et al. (2014) who illustrated this example did not characterise the dark (low atomic contrast) matrix around the SiC fragments, so it is unclear if SiC occurs in a void or a light element matrix like carbon (cf. Yang et al., 2007). Nor did they document that the composition of the spinel in contact with SiC reacted locally to the low redox state imposed by SiC. Angular SiC fragments, potentially in voids, are not what we expect from *"in-situ"* SiC inclusions that were trapped at high pressure under convecting mantle conditions. That the angular SiC grains are UHP phases as asserted can only be entertained if the host chromite is proven to have crystallised initially in the orthorhombic calcium ferrite (CF) structure (Chen et al., 2003). Liang et al. (2014) failed to demonstrate this.

Many other phases considered to be mantle derived also raise issues. For example, Yang et al. (2015) recovered from the Ray Iz ophiolite ultra-reduced phase populations including metallic Zr, Ta, Ta-Co alloys, metallic Cr, and tungsten carbide aggregates. At 1600K metallic Zr is around 7 orders more reduced than SiC (Barin, 1995), so would we now allocate the Ray Iz ophiolite a relative $fO_2$ of IW-15? As for metallic Ta, there is no natural process known that would separate the geochemical twins Nb and Ta to the extent that pure Ta metal results. The Nb-Ta ratio of Earth's mantle is ~ 14 (Münker et al., 2003; Witt-Eickschen and O'Neill, 2005), hence large quantities of Nb would have to "disappear" before pure Ta could form. The phase more stable would be metallic Nb, not Ta, since Nb is more siderophile than Ta (Wade and Wood, 2001). The WC aggregates in Figure 1H and 1I are also dubious. The matrix to the euhedral WC grains appears to be metallic

Co, a metal that is used industrially to sinter WC crystals to carbide metal. We find it disturbing to note that both WC images are identical (i.e. from the same aggregate), yet that they were reported as having been derived from two ophiolites more than 4600 km apart: Figure 1H from Ray Iz in the Polar Urals (Yang et al., 2015), Figure 1I from Luobusa in Tibet (Fang et al., 2009).

The ferroan ringwoodite (Rw) skeletons in Figure 1J, now named ahrensite, from a siliceous pumice in Spain (Díaz-Martinez and Ormö, 2003; Glazovskaya and Feldman, 2010) are not reduced. We do include them nonetheless in our compilation to illustrate that UHP phases may also nucleate metastably outside their stability fields; as do coesite (Bouška and Feldman, 1994), stishovite (Shveikin et al., 2015), and diamond (Angus and Hayman, 1988; Farré-de-Pablo et al., 2018). Before one speculates on UHP histories of ophiolites, one should document the crystal shapes of the UHP phases to help judge the reader if they could be metastable in origin.

*Can ultra-reduced phases be stabilised by $CH_4$-$H_2$ fluids?*

Griffin et al. (2016b; 2019; 2020), Xiong et al. (2017), and Bindi et al. (2019) documented skeletal corundum-hibonite-grossite fragments from the Kishon River at the foothills of the Mt. Carmel basaltic complex, northern Israel. The aggregates carry ultra-reduced phases like TiN osbornite, $Ti_2O_3$ tistarite, V metal, (V,Al) alloys, and V hydrides (Fig. 1E,F). Although the fragments have nothing to do with ophiolites, they do fit in this paper because the mode proposed of their origin - infiltration of the mantle sources by ultra-reduced $CH_4$-$H_2$ fluids - was recently applied to stabilise ultra-reduced phases in ophiolites as well (Xiong et al., 2017).

We test by mass balance how much $CH_4$-$H_2$ fluid would have to be infiltrated in a mantle source to reduce all FeO and stabilise SiC. As infiltration fluid we choose a C-H-O composition in equilibrium with SiC synthesised by Matveev et al. (1997). These authors combusted organic C-H-O compounds to C-H-O fluids at 1273K and 2 GPa in the presence of solid state oxygen buffers, including SiC-$SiO_2$-C (Fig. 7). Fluids in equilibrium with SiC and graphite were analysed by gas chromatography and mass spectrometry and had 91.4 ± 0.5 mole% $CH_4$, 1.9 ± 0.1 mole% $C_2H_6$, 6 ± 0.4 mole% $H_2$ with traces of $H_2O$ at the detection limit. The molar H-O ratio was 900 ± 550 (n = 3).

As for the mantle material, we choose a mantle composition with 8 wt.% FeO (Palme and O'Neill, 2014). One cubic meter of that material contains 3900 moles FeO. The bulk reduction reaction with the SiC fluid composition specified above would then be

$$1.94\ FeO + 0.06\ H_2 + 0.94\ CH_4 = 1.94\ Fe° + 1.94\ H_2O + 0.94\ C \qquad (2)$$

To simplify things we allot $C_2H_6$ to $CH_4$. To reduce 3900 moles FeO to Fe° ca. 2000 moles of $CH_4$-$H_2$ (94/6) fluid must be infiltrated. We follow Griffin et al. (2019) and assume the fluid was infiltrated at 0.7 GPa near the MOHO. We set the infiltration temperature to 1600K appropriate for a time of intense magmatic activity at Mt. Carmel. At these P-T conditions the volume of 2000 moles $CH_4$-$H_2$ (94/6) fluid is approximated with an MRK EoS (Anderson and Crerar, 1993) to ~ 0.1 $m^3$. The molar volume is around 48 $cm^3$.

A fluid-rock volume ratio of 0.1 seems reasonable but note that the infiltration depth (near the MOHO) is an *ad hoc* estimate by Griffin et al. (2019) unconstrained by independent evidence. Had the hypothetical fluid been infiltrated at shallower depth the fluid-rock ratio would increase dramatically with falling

This is the peer-reviewed, final accepted version for American Mineralogist, published by the Mineralogical Society of America.
The published version is subject to change. Cite as Authors (Year) Title. American Mineralogist, in press.
DOI: https://doi.org/10.2138/am-2021-7612. http://www.minsocam.org/


pressure and would soon become unrealistic (Fig. 8). More important, however, are the following concerns:

- How was it possible that the mantle that produced basalts with 12 wt.% FeO + $Fe_2O_3$ (Kaminchik et al., 2014) emanated ultra-reduced $CH_4$-$H_2$ fluids? Alkali basalts are oxidized around FMQ+1 and their equilibrium volatiles are $H_2O$ and $CO_2$. Griffin et al. (2020) realised that problem but circumvented it by stating (rather *ad hoc*) the fluid infiltration episode was unrelated to the alkali basaltic volcanism. No reasons are given for that assertion.

- Corundum (Fig. 1F) and $(Al,Cr)_2O_3$ solid solutions afford temperatures in excess of 2270K (Muan and Somiya, 1959). Phases in the system $Al_2O_3$-$Ti_2O_3$-$TiO_2$ including tistarite $Ti_2O_3$ crystallise at around 1900K (Jung et al., 2009). Hibonite-grossite-corundum assemblages record minimum temperatures around 1875K if they once coexisted with melt (cf. Jerebtsov and Mikhailov, 2001). Metallic V reported by Bindi et al. (2019) has a liquidus temperature of 2180K (Murray 1989). Temperatures in that range are unrealistic for a Cretaceous volcanic province. The MgO contents of primitive Mt. Carmel basalts (Kaminchik et al., 2014), around 13 to 14 wt.% plus perhaps 0.5 wt.% $H_2O$ + $CO_2$, constrain the liquidus temperature to around 1520K (Helz and Thornber, 1987).

- When sapphire crystals are entrained as xenocrysts in alkali basalts they react to spinel via $Al_2O_3 + (MgO,FeO)_{basalt} = (Mg,Fe)Al_2O_4$. The reaction is fast (Baldwin et al., 2017). So why are the corundum fragments not mantled by spinel coronas if they were carried to the surface by FeO rich hot alkali basalts, for a distance of 25 to 30 km?

- Why should corundum-hibonite-grossite-tistarite aggregates be skleletal (Fig. 1F and Xiong et al., 2017) if they crystallised from natural basalts or their mantle sources at depth?

- Griffin et al. (2020) believe they identified relicts of the reducing fluid. They assert that voids in their Mt. Carmel fragments were filled originally by $H_2$ - a rather adventurous proposition when by definition a void is empty.

- The vanadium metal and (V,Al) alloys (Fig. 1E and Griffin et al., 2019) may be small but by what natural process were V oxide components enriched to up to 100 wt.% then reduced to their metal states, when alkali basalts contain ~ 250 to 300 ppm V as oxide component (Doe, 1997) and ca. 15 wt.% $Al_2O_3$? What type of magmatic fractionation process selectively enriched V and Al?

- Why were no ultra-reduced, FeO-free silicates picked up by the alkali basalts of Mt. Carmel if the mantle source was that reduced?

We agree with Litasov et al. (2019) that the skeletal corundum-rich fragments of the Kishon river locality are anthropogenic in origin. They could be relicts/refuse of the aerospace and/or medical implant industry where Ti-Al-V light metal alloys are cast into refractory moulds composed of fused alumina and zirconia and occasionally yttria. After freezing, the metal-contaminated mould is being knocked off and disposed. The metal itself is melted from constituents in the form of pure Ti metal sponge and an Al-V pre-alloy where large chunks are typically subjected to a process of hydridation - dehydridation for easier comminution. Melting and casting of Ti-Al-V alloys take place under vacuum or protective atmosphere since Ti-Al-V alloys are extremely reactive with air. Even in an already frozen hot stage the alloys easily react with $N_2$ to form nitrides (A. Bouvier and K. Rabitsch, pers. comm. 2020).

Hydrogenation and nitridation may stabilise metal hydrides and nitrides - phases that were described by Griffin et al. (2019) and Bindi et al. (2019) and "sold" as minerals. We propose that the Kishon River aggregates are fragments of zirkonia-lined alumina casting moulds that were infiltrated by Ti-Al-V melts. Following Litasov et al. (2018) we rule out a natural origin and a genetic connection to the Cretaceous Mt. Carmel basalts.

## IMPLICATIONS

Ultra-reduced phases such as SiC or Fe-Si alloys would have no chance of forming or surviving for any length of time in FeO bearing asthenospheric mantle. Silicon carbide, arguably the most prominent among the ultra-reduced phases in ophiolites, is unstable both chemically and texturally. Silicon carbide is incompatible with almost every aspect of known mantle mineralogy. Based on a few exotic phases of doubtful provenance it does not seem target-oriented to rewrite the history of ophiolites so fundamentally as proposed by Griffin et al. (2016a) and Xiong et al. (2015).

That diamonds and ultra-reduced phases are found in the same heavy mineral concentrates does not mean a genetic link must exist between these phases and ophiolites. The diamonds could be contamination, notably those with Mn-Ni-Co metal melt inclusions (Yang et al., 2014; 2015; Griffin et al., 2016a), diamonds with trace element signatures identical to Russian and Chinese synthetics (Litasov et al., 2019), and diamonds with (young) 1B nitrogen aggregation states.

Ballhaus et al. (2017) noted that some ultra-reduced phases in ophiolite concentrates resemble minerals in fulgurites. They exposed basalts and ultramafic mantle rocks to electric discharges at 9.9 kV and 30 kA at temperatures in excess

of 6000K simulating temperatures when lightning bolts strike solid rocks. At 6000K lithologies are vaporised to plasmas. The first and highest temperature precipitates of the plasmas were silicon, Fe-Si silicides, SiC, metals, metal alloys, and amorphous carbon, exactly the phases found in ophiolite concentrates. There is no reasonable reason argument that can be made to oppose analogies to fulgurites (cf. Griffin et al., 2018; Yang et al., 2018; Xiong et al., 2019):

- plasmas produce perfectly rounded spherules when they are quenched in air (Genareau et al., 2015), and these spherules are found in both ophiolite concentrates (Yang et al., 2015; Griffin et al., 2016a), in surface sediments of ophiolites (Zuxiang, 1984), and as ejecta of the Ballhaus et al. (2017) experiments;
- plasmas quench extremely rapidly and produce skeletal crystal morphologies as those compiled in Figure 1 (cf. Essene and Fisher, 1986); and
- plasmas solve the redox paradox as they may condense within any lithology on any type of surface, regardless of the redox states of the rocks within which they occur.

Lightning bolts are one hypothesis among others. Diamonds, SiC, and Fe-Si alloys may well form metastably at low temperature and pressure (Angus and Hayman, 1988; Ishimaru et al., 2009; Schmidt et al., 2014; Shiryaev and Gaillard, 2014; Farré-Paolo et al., 2018; Pujol-Solà et al., 2020). In addition, there is a certain probability that many ultra-reduced phases reported from ophiolites and elsewhere simply arise from contamination during sample handling and lack of due diligence by the original authors in looking for possible sources of contamination before ruling it out.

This is the peer-reviewed, final accepted version for American Mineralogist, published by the Mineralogical Society of America.
The published version is subject to change. Cite as Authors (Year) Title. American Mineralogist, in press.
DOI: https://doi.org/10.2138/am-2021-7612. http://www.minsocam.org/


## ACKNOWLEDGEMENTS

We thank the machine shops of the Geoscience Institute for keeping the experimental equipment in excellent running order. Matthias Gottschalk and Jamie Connolly greatly helped in checking the PVT properties calculated for $CH_4$-$H_2$ fluids. Alexander Bouvier and Kurt Rabitsch of the Treibach Industrie AG directed the first author to process technologies used in the production of Ti-Al-V light metal casts. Hanna Cieszynski kindly imaged selected textures with FE-SEM at high resolution. Insightful comments by Hugh O'Neill and an anonymous reviewer, as well as efficient editorial handing by Fabrizio Nestola are greatly appreciated. Funded by the German Science Foundation (DFG) through grant Ba 964/37 to Chris Ballhaus, through a Georg Forster Prize awarded by the Alexander von Humboldt Foundation to Hassan M. Helmy, and through a Heisenberg Professorship to Raúl O.C. Fonseca by the DFG via grant number FO 698/11-1.

## REFERENCES CITED

Anderson, G.M., and Crerar, D.A. (1993) Thermodynamics in Geochemistry. The Equilibrium Model. Oxford University Press, 588 p.

Angus, J.C., and Hayman, C.C. (1988) Low-pressure, metastable growth of diamond and "diamondlike" phases. Science, 241, 913-921.

Baldwin, L.C., Tomaschek, F., Ballhaus, C., Gerdes, A., Fonseca, R.O.C., Wirth, R., Geisler, T., and Nagel, T. (2017) Petrogenesis of alkaline basalt-hosted sapphire megacrysts. Petrological and geochemical investigations of in situ sapphire occurrences from the Siebengebirge Volcanic Field, Germany. Contributions to Mineralogy and Petrology, 172, 43, DOI 10.1007/s00410-017-1362-0.

Ballhaus, C., Berry, R.F., and Green D.H. (1991) Experimental calibration of the olivine-orthopyroxene-spinel oxygen barometer - implications for oxygen fugacity in the Earth's upper mantle. Contributions to Mineralogy and Petrology, 107, 27-40.

Ballhaus, C., Wirth, R., Fonseca, R.O.C., Blanchard, H., Pröll, W., Bragagni, A., Nagel, T., Schreiber, A., Dittrich, S., Thome, V., Hezel, D.C., Below, R., and Cieszynski, H. (2017) Ultra-high pressure and ultra-reduced minerals in ophiolites may form by lightning strikes. Geochemical Perspectives Letters, 5, 42-46.

Ballhaus, C., Fonseca, R.O.C., and Bragagni, A. (2018a) Reply to Comment on “Ultra-high pressure and ultra-reduced minerals in ophiolites may form by lightning strikes” by Griffin et al. (2018): No evidence for transition zone metamorphism in the Luobusa ophiolite. Geochemical Perspectives Letters, 7. doi: 10.7185/geochemlet.1810.

Ballhaus, C., Blanchard, H., Fonseca, R.O.C., and Bragagni, A. (2018b) Reply 2 to comment on “Ultra-high pressure and ultra-reduced minerals in ophiolites may form by lightning strikes". Geochemical Perspectives Letters, 8, 8-10 | doi: 10.7185/geochemlet.1821.

Barin, I. (1995) Thermochemical data of pure substances I + II, 3rd edition. VCH Verlagsgesellschaft, 1885 p.

Berry, A.J., and O'Neill, H.St.C. (2004) A XANES determination of the oxidation state of chromium in silicate glasses. American Mineralogist, 89, 790-798.

Bindi, L., Cámara, F., Griffin, W.L., Huang, J.X, Gain, S.E.M, Toledo, V., and O'Reilly, S.Y. (2019) Discovery of the first natural hydride. American Mineralogist, 104, 611–614.

Bouška, V., and Feldman, V.I. (1994) Terrestrial and lunar, volcanic and impact glasses, tektites, and fulgurites. In Marfunin, A.S. (ed.) Advanced Mineralogy 258-265. doi:10.1007/978-3-642-78523-8.

Bryan, W.B. (1972) Morphology of quench crystals in submarine basalts. Journal of Geophysical Research, 77, 5812-5819.

Chen, M., Shu, J., Mao, H.K., Xie, X., and Hemley, R.J. (2003) Natural occurrence and synthesis of two new postspinel polymorphs of chromite. PNAS, 100, 14651-14654.

Das, S., Basu, A.R., and Mukherjee, B.K. (2017) In situ peridotitic diamond in Indus ophiolite sourced from hydrocarbon fluids in the mantle transition zone. Geology, 45, 755–758.

532 Díaz-Martinez, E., and Ormö, J. (2003) An alternative hypothesis for the origin of
533 ferroan ringwoodite in the pumice of El Gasco (Cáceres, Spain). Lunar and
534 Planetary Science XXXIV, 1318.

535 Dilek, Y., and Furnes, H. (2014) Ophiolites and their origins. Elements, 10, 93–
536 100.

537 Dobrzhinetskaya, L.F., Wirth, R., Yang, J., Hutcheon, I.D., Weber, P.K., and
538 Green II, H.W. (2009) High-pressure highly reduced nitrides and oxides from
539 chromitite of a Tibetan ophiolite. PNAS, 106, 19233-19238.

540 Doe, B.R. (1997) Geochemistry of oceanic igneous rocks — ridges, islands, and
541 arcs — with emphasis on manganese, scandium, and vanadium. International
542 Geological Review, 39, 1053-1112.

543 Donaldson, C.H. (1976) An experimental investigation of olivine morphology.
544 Contributions to Mineralogy and Petrology, 57, 187-213.

545 Essene, E.J., and Fisher, D.C. (1986) Lightning strike fusion: Extreme reduction
546 and metal-silicate liquid immiscibility. Science, 234, 189-193.

547 Fang, Q., Bai, W., Yang, J., Xu, X., Li., G. Shi, N., Xiong, M., and Rong, H.
548 (2009) Qusongite (WC): A new mineral. American Mineralogist, 94, 387-390.

549 Farré-de-Pablo, J., Joaquín, A., Proenza, J.A., González-Jiménez, J.M., Garcia-
550 Casco, A., Colás, V., Roqué-Rossell, J., Camprubí, A., and Sánchez-Navas, A.
551 (2018) A shallow origin for diamonds in ophiolitic chromitites. Geology, 47, 75-
552 78.

553 Gao Z., and Lu H. (2016) Preparation of Ti-Al-V alloys by aluminothermic
554 reaction. In: Li L. et al. (eds) Energy Technology 2016. Springer, Cham.
555 https://doi.org/10.1007/978-3-319-48182-1_8.

Genareau, K., Wardman, J.B., Wilson, T.M., McNutt, S.R., and Izbekov, P. (2015) Lightning-induced volcanic spherules. Geology, 43, 319–322.

Glazovskaya, L.I., and Feldman, V.I. (2010) Petrology of ringwoodite bearing pumices of the El Gasco region, West Spain. European Planetary Science Congress EPSC2010-75 (abstract).

Golubkova, A., Schmidt, M.W., and Connolly, J.A.D. (2016) Ultra-reducing conditions in average mantle peridotites and in podiform chromitites: a thermodynamic model for moissanite (SiC) formation. Contributions to Mineralogy and Petrology, 171, doi: 10.1007/s00410-016-1253-9.

Griffin, W.L., Afonso, J.C., Belousova, E.A., Gain, S.E., Gong, X.-H., González-Jiménez, J.M., Howell, D., Huang, J.-X., McGowan, N., Pearson, N.J., Satsukawa, T., Shi, R., Williams, P., Xiong, Q., Yang, J.-S., Zhang, M., and O'Reilly, S.Y. (2016a) Mantle recycling: Transition zone metamorphism of Tibetan ophiolitic peridotites and its tectonic implications. Journal of Petrology, 57, 655-684.

Griffin, W.L., Gain, S.E.M., Adams, D.T., Huang, J-X., Saunders, M., Toledo, V., Pearson, N.J., and O'Reilly S.Y. (2016b) First terrestrial occurrence of tistarite ($Ti_2O_3$): Ultra-low oxygen fugacity in the upper mantle beneath Mount Carmel, Israel. Geology 44, 815-818.

Griffin, W.L., D. Howell, D., Gonzalez-Jimenez, J.M., Xiong, Q., and O'Reilly, S.Y. (2018) Comment on "Ultra-high pressure and ultra-reduced minerals in ophiolites may form by lightning strikes" by Ballhaus et al. (2017): Ultra-high pressure and super-reduced minerals in ophiolites do not form by lightning strikes. Geochemical Perspectives Letters, 7, 1-2 | doi: 10.7185/geochemlet.1809.

Griffin, W.L., Gain, S.E.M., Huang, J.-X., Saunders, M., Shaw, J., Toledo, V., and O'Reilly, S.Y. (2019) A terrestrial magmatic hibonite-grossite-vanadium

assemblage: Desilication and extreme reduction in a volcanic plumbing system, Mount Carmel, Israel. American Mineralogist, 104, 207–219.

Griffin, W.L., Gain, S.E.M., Cámara, F., Bindi, L., Shaw, J., Alard, O., Saunders, M., Huang, J.-X., Toledo, V., and O'Reilly, S.Y. (2020) Extreme reduction: Mantle-derived oxide xenoliths from a hydrogen-rich environment. Lithos, https://doi.org/10.1016/j.lithos.2020.105404.

Haggerty, S.E. (1978) The redox state of planetary basalts. Geophysical Research Letters, 5, 443-446.

Helz, R.T., and Thornber, C.R. (1987) Geothermometry of Kilauea Iki lava lake, Hawaii. Bulletin Volcanology, 49, 651-66.

Howell, D., Griffin W.L., Yang, S., Gain S., Stern, R.A., Huang, J.-X., Jacob, D.E., Xu, X., Stokes, A.J. O'Reilly, S.Y., and Pearson, N.J. (2015) Diamonds in ophiolites: Contamination or a new diamond growth environment? Earth and Planetary Science Letters, 430, 284–295.

Ishimaru, S., Arai, S., and Shukuno, H. (2009) Metal-saturated peridotite in the mantle wedge inferred from metal-bearing peridotite xenoliths from Avacha volcano, Kamchatka. Earth and Planetary Science Letters, 284, 352–360.

Jerebtsov, D.A., and Mikhailov, G.G. (2001) Phase diagram of $CaO$-$Al_2O_3$ system. Ceramics International, 27, 25-28.

Jung, I.-H., Eriksson, G., Wu, P., and Pelton, A. (2009) Thermodynamic modeling of the $Al_2O_3$–$Ti_2O_3$–$TiO_2$ system and its applications to the Fe–Al–Ti–O inclusion diagram. ISIJ International, 49, 1290–1297.

Kaminchik, J., Segev, A., and Katzir, Y. (2014) The origin of intraplate alkaline mafic magmatism in continental shelves: lavas and xenoliths from the Upper

Cretaceous volcanoes of Mt Carmel. Geological Survey of Israel Publication, 9, 99 p.

Kelemen, P.B., Dick, H.J.B., and Quick, J.E (1992) Formation of harzburgite by pervasive melt/rock reaction in the upper mantle. Nature, 358, 635-641.

Klemme, S., and O'Neill, H.St.C. (2000) The near-solidus transition from garnet lherzolite to spinel lherzolite. Contributions to Mineralogy and Petrology, 138, 237-248.

Li, J.-P., O'Neill, H.St.C, and Seifert, F. (1995). Subsolidus phase relations in the system MgO—$SiO_2$—Cr—O in equilibrium with metallic Cr, and their significance for the petrochemistry of chromium. Journal of Petrology, 36, 107-132.

Liang, F., Xu, Z., and Thao, J. (2014) In-situ moissanite in dunite: deep mantle origin of mantle peridotite in Luobusa ophiolite, Tibet. Acta Geologica Sinica, 88, 517-529.

Litasov, K.G., Kagi, H., and Bekker, T.B. (2018). Enigmatic super-reduced phases in corundum from natural rocks: Possible contamination from artificia abrasive materials or metallurgical slags. Lithos, 340, 181-190.

Litasov K.G., Kagi, H., Voropaev, S.A., Hirata, T., Ohfuji, H., and Ishibashi, H. (2019). Comparison of enigmatic diamonds from the Tolbachik arc volcano (Kamchatka) and Tibetan ophiolites: Assessing the role of contamination by synthetic materials. Gondwana Research, 75, 16-27.

Matveev, S., Ballhaus, C., Fricke, K., Truckenbrodt, J., and Ziegenbein, D. (1997) Volatiles in the Earth's mantle: I. Synthesis of CHO fluids at 1273K and 2.4 GPa. Geochimica et Cosmochimica Acta, 61, 3081-3088.

Miyashiro, A. (1973) The Troodos ophiolite complex was probably formed in an island arc. Earth and Planetary Science Letters, 19, 218-224.

Muan, A., and Somiya, S. (1959) Phase equilibrium studies in the system iron oxide-$Al_2O_3$-$Cr_2O_3$. Journal of the American Ceramic Society, 42, 603-613.

Münker, C., Pfänder, J.A., Weyer, S., Büchl, A., Kleine, T., and Mezger, K. (2003) Evolution of planetary cores and the Earth-Moon system from Nb/Ta systematics. Science, 301, 84-87.

Murray, J. L. (1989). Al-V (aluminum-vanadium). Bulletin of Alloy Phase Diagrams, 10, 351–357. doi:10.1007/bf02877591.

Nicholas, A. (1999) Les Montagnes sous la Mer. Editions du B.R.G.M., Orléans.

O'Neill, H.St.C. (1987) The quartz-fayalite-iron and quartz-fayalite-magnetite equilibria and the free energies of formation of fayalite ($Fe_2SiO_4$) and magnetite ($Fe_3O_4$). American Mineralogist, 72, 67-75.

O'Neill, H.St.C., and Wall, V.J. (1987) The olivine-orthopyroxene-spinel oxygen geobarometer, the nickel precipitation curve, and the oxygen fugacity of the Earth's Upper Mantle. Journal of Petrology, 28, 1169-1191.

O'Neill, H.St.C., Pownceby, M.I., and McCammon, C.A. (2003) The magnesiowüstite - iron equilibrium and its implications for the activity-composition relations of $(Mg,Fe)_2SiO_4$ olivine solid solutions. Contributions to Mineralogy and Petrology, 146, 308–325.

O'Neill, H.St.C., and Palme, H. (2014) Cosmochemical estimates of mantle composition. In: Treatise on Geochemistry 2nd Edition
http://dx.doi.org/10.1016/B978-0-08-095975-7.00201-1

Pearce, J.A., and Robinson, P.T. (2010) The Troodos ophiolitic complex probably formed in a subduction initiation, slab edge setting. Gondwana Research, 18, 60–81.

Pujol-Solà, N., Garcia-Casco, A., Proenza, J.A., González-Jiménez, J.M., del Campo, A., Colás, V., Canals, A., Sánchez-Navas A., and Roqué-Rossell, J. (2020) Diamond forms during low-pressure serpentinization of oceanic lithosphere. Geochemical Perspectives Letters, in press.

Putnis, A. (2002) Mineral replacement reactions: from macroscopic observations to microscopic mechanisms. Mineralogical Magazine, 66, 689–708.

Robertson, A.H.F. (2002) Overview of the genesis and emplacement of Mesozoic ophiolites in the Eastern Mediterranean Tethyan region. Lithos, 65, 1-67.

Robinson, P.T., Bai, W.J., Malpas, J., Yang, J.-S., Zhou, M.-F., Fang, Q.-S., Hu, X.-F., Cameron, S., and Staudigel, H. (2004) Ultra-high pressure minerals in the Luobusa Ophiolite, Tibet, and their tectonic implications. Geological Society of London, Special Publication, 226, 247–271.

Rohrbach, A., Ballhaus, C., Golla-Schindler, U., Ulmer, P., Kamenetsky, V.S., and Kuzmin, D.V. (2007) Metal saturation in the upper mantle. Nature 449, 456-458.

Schmidt, M.W., Gao, C., Golubkova, A., Rohrbach, A., and Connolly, J.A.D. (2014) Natural moissanite (SiC) - a low temperature mineral formed from highly fractionated ultra-reducing COH-fluids. Progress in Earth and Planetary Science, 1, 27. doi.org/10.1186/s40645-014-0027-0

Schreiber, H.D. (1979) Experimental studies of nickel and chromium partitioning into olivine from synthetic basaltic melts. 10th Lunar and Planetary Science Conference 509-516.

Shiryaev, A.A., and Gaillard, F. (2014). Local redox buffering by carbon at low pressures and the formation of moissanite–natural SiC. European Journal of Mineralogy, 26, 53-59.

Stubican, V.S., and Greskovich, C. (1975) Trivalent and divalent chromium ions in spinel. Geochimica et Cosmochimica Acta, 39, 875-881.

Sung, C.-M., and Tai, M.-F. (1997) Reactivities of transition metals with carbon: Implications to the mechanism of diamond synthesis under high pressure. International Journal of Refractory Metals and Hard Materials, 15, 237–256.

Sutton, S.R., Jones, K.W., Gordon, B., Rivers, M.L., Bajt, S., and Smith, J.V. (1993) Reduced chromium in olivine grains from lunar basalt 15555: X-ray Absorption Near Edge Structure (XANES). Geochimica et Cosmochimica Acta, 57, 461-468.

Tan, X. (2014) Catalyst alloys processing. JOM 66, 2176–2185. doi.org/10.1007/s11837-014-0984-1

Taylor, W.R., and Green, D.H. (1989) The role of reduced C-H-O fluids in mantle partial melting. In: Kimberlites and Related Rocks: Their Composition, Occurrence, Origin and Emplacement (Ross J., Editor). Geological Society of Australia, Special Publication, 14, 592-602.

Ulmer, G.C., Grandstaff, D.E., Woermann, E., Göbbels, M., Schönitz, M., and Woodland, A.B. (1998) The redox stability of moissanite (SiC) compared with metal-metal oxide buffers at 1773 K and at pressures up to 90 kbar. Neues Jahrbuch für Mineralogie Abhandlungen, 172, 279 - 307

Wade, J., and Wood, B. (2001) The Earth's ‘missing ’niobium may be in the core. Nature, 409, 75–78 (2001). https://doi.org/10.1038/35051064

Wirth, R. (2009) Focused Ion Beam (FIB) combined with SEM and TEM: advanced analytical tools for studies of chemical composition, micro-structure and crystal structure in geomaterials on a nanometer scale. Chemical Geology, 261, 217–229.

Wiser, N.M., and Wood, B.J. (1991) Experimental determination of activities in Fe−Mg olivine at 1400 K. Contributions to Mineralogy and Petrology, 108, 146–153.

Witt-Eickschen, G., and O'Neill, H.St.C (2005) The effect of temperature on the equilibrium distribution of trace elements between clinopyroxene, orthopyroxene, olivine and spinel in upper mantle peridotite. Chemical Geology, 221, 65-101.

Xiong, F., Yang, J., Robinson, P.T., Xu, X., Liu, Z., Li, Y., Li, J., and Chen, S. (2015) Origin of podiform chromitite, a new model based on the Luobusa ophiolite, Tibet. Gondwana Research, 27, 525-542.

Xiong, Q., Griffin, W.L., Huang, J.-X., Gain, S.E.M., Toledo, V., Pearson, N.J., and O'Reilly, S.Y. (2017) Super-reduced mineral assemblages in “ophiolitic” chromitites and peridotites: the view from Mount Carmel. European Journal of Mineralogy DOI: 10.1127/ejm/2017/0029-2646.

Xiong, F., Liu, Z., Kapsiotis, A., Yang, J., Lenaz, D., and Robinson, P.T. (2019) Petrogenesis of lherzolites from the Purang ophiolite, Yarlung-Zangbo suture zone, Tibet: origin and significance of ultra-high pressure and other ‘unusual ’minerals in the Neo-Tethyan lithospheric mantle. International Geological Review, https://doi.org/10.1080/00206814.2019.1584771.

Xu, X., Yang, J., Robinson, P.T., Xiong F., Ba, D., and Guo, G. (2015) Origin of ultrahigh pressure and highly reduced minerals in podiform chromitites and

associated mantle peridotites of the Luobusa ophiolite, Tibet. Gondwana Research, 27, 686–700.

Xu, X., Cartigny, P., Yang J., Dilek Y., Xiong F., and Guo, G. (2017) Fourier transform infrared spectroscopy data and carbon isotope characteristics of the ophiolite-hosted diamonds from the Luobusa ophiolite, Tibet, and Ray-Iz ophiolite, Polar Urals. Lithosphere, 10, 156–169.

Yang, J., Dobrzhinetskaya, l.F., Bai, W.J., Junfeng Zhang, J., and Green II, H.W. (2007) Diamond and coesite-bearing chromitites from the Luobusa ophiolite, Tibet. Geology, 35, 875–878.

Yang, J., Robinson, P.T., and Dilek, Y. (2014) Diamonds in ophiolites: A little-known diamond occurrence. Elements, 10, 127–130.

Yang, J., Meng, A., Xu, X., Robinson, P.T., Dilek, Y., Makeyev, A.B., Wirth, R., Wiedenbeck, M., Griffin, W.L., and Cliff, J. (2015) Diamonds, native elements and metal alloys from chromitites of the Ray-Iz ophiolite of the Polar Urals. Gondwana Research, 27, 459–485.

Yang, J.S., Trumbull, R.P., Robinson, P.T., Xiong, F.H., and Lian, D.Y. (2018) Comment 2 on “Ultra-high pressure and ultra-reduced minerals in ophiolites may form by lightning strikes”. Geochemical Perspectives Letters, 8, 6-7.

Zhou, L., Jia, X.-P., Ma, H.A., Zheng, Y.-J., and Li, Y.-T. (2009) Industrial diamonds grown in $Ni_{70}Mn_{25}Co_5$–graphite–sulfur system under HPHT. Chinese Physics, B18, 333-338.

Zuxiang, Y. (1984) Two new minerals gupeiite and xifengite in cosmic dusts from Yanshan. Acta Petrologica Mineralogica et Analytica, 3 (abstract).

748 Figure Captions

749 Figure 1. Textures of ultra-reduced minerals in ophiolites and Kishon River
750 aggregates.

751 A - an Fe-Si-Ti-P symplectite from Luobusa documented by Robinson et al.
752 (2004). Tubular inclusions enriched in metallic Ti and P but essentially Fe-Si
753 alloys. Texturally it seems they exsolved from the Fe-Si matrix and were preserved
754 *in-situ* because of rapid quenching.

755 B and C - details of a zonar Fe-Ti-Si grain aggregate recovered from a bulk
756 chromite sample from Luobusa (Yang et al., 2007; Dobrzhinetskaya et al. 2009). In
757 the original Figure (Yang et al., 2007) the Fe-Ti symplectites are surrounded by
758 rims of Fe-Ti alloy, native Ti, pseudomorphs of coesite after stishovite, and
759 kyanite. Dobrzhinetskaya et al. (2009) documented within coesite of this aggregate
760 nanoscale Ti nitrides.

761 D - an Ni-(Fe-Cr)-C carbide grain with skeletal Cr carbide needles, recovered from
762 concentrates of a 500 kg chromitite bulk sample from Luobusa (Robinson et al.,
763 2004).

764 E and F - V-Al, TiN, and $Ti_2O_3$ skeletons with metallic V and a vanadium hydride
765 ($VH_2$) grain attached, in corundum (co) matrix (Griffin et al., 2016b; 2019; Bindi et
766 al., 2019). For discussion of these fragments see text.

767 G - a BSE image of "*in-situ*" SiC fragments in chromite from Luobusa (Liang et
768 al., 2014), claimed to be lower mantle derived. The dark (low atomic number
769 contrast) matrix around the SiC fragments is not specified, potentially a void or
770 carbon. Note that the host chromite is not stable at pressures prevalent in the ower
771 mantle (Chen et al., 2003).

H and I - aggregates of euhedral "qusongite" (WC) grains in a Co metal matrix (Fang et al., 2009; Yang et al. 2015). The two photos are identical (cf. one WC grain outlined in red for orientation) although they supposedly come from different WC aggregates of two different ophiolites (Ray Iz and Luobusa) 4600 km apart (see text).

J - skeletal ferroan ringwoodite (Rw), now ahrensite, in a glassy pumice from Spain (Díaz-Martinez and Ormö, 2003). Although ringwoodite is not an ultra-reduced mineral this photo is included in the compilation of disequilibrium morphologies to illustrate that UHP phases need not be UHP but can grow metastable at much lower pressures than their equilibrium pressures.

All images modified from the original sources to avoid copyright conflicts.

Figure 2. Oxygen fugacities imposed by the assemblages fayalite-magnetite-quartz (FMQ), iron-wüstite (IW), $Ti_2O_3$-$TiO_2$, and SiC-$SiO_2$-C. The FMQ and IW buffers are from O'Neill (1987), the other equilibria were calculated using thermodynamic data by Barin (1995). The dashed line approximates experimental $fO_2$ conditions as described in the text. All calculations for 1 atm. Redox gradient at 1600K marked by arrows. Higher pressure changes absolute fugacities but the $fO_2$ differences among the buffers and the 1/T - ($\Delta$H / RT) slopes remain largely unaffected by pressure.

Figure 3. Backscattered images of the experimental runs. A - BSE image illustrating reduction rims around two olivine ($Fo_{89}$) relicts that reacted with SiC (cr-6); positions of three FIB foils marked in red. B - reduced olivine with exsolved Fe-Ni metal, in C and D element maps of Ni and Mg; most magnesian olivine

marked by arrows. E and F - relict Bushveld chromite surrounded by reduced spinel slightly lower in atomic number contrast; bright veinlets are (Fe,Cr) metal. G - zoned Al-spinel surrounded by silicate melt (now glass). H - spinel aggregate with chromite cores veined by (Fe,Cr) metal; one FIB foil marked in red, white frame mapped for element distribution (Fig. 4). I - SiC grain with $SiO_2$ reaction rim. J - $SiO_2$ reaction rim around SiC in high resolution. K - Fe-Cr±Si±C metal grain (former melt?) exsolved to Cr, Si, and Fe enriched fractions; red frame mapped for element distributions.

Figure 4. Element maps of the chromite aggregate of Figure 3H illustrating compositional effects upon reduction by SiC. Warmer colors indicate higher concentrations. For position see frame in Fig. 3H.

Figure 5. TEM images of run products. A - forsterite (~ $Fo_{96}$) with Fe-Ni metal inclusions in reduction rim around relict olivine (cf. Fig. 3A); the Fast Fourier Transform (FFT) as inset to illustrate that the metal inclusions are cubic α-(Fe,Ni). B - reduced spinel with cubic (Fe,Cr)° metal and cubic ferroan periclase inclusions marked in red (FFT as inset). C - euhedral (Fe,Cr)° metal grains in reduced spinel. D - bright field image of defect-rich spinel, FFT to illustrate that the spinels are cubic; the dark schlieren are dislocations.

Figure 6. Chromite compositions (atomic ratios). Black symbols illustrate oxidised LG-1 Bushveld chromites (~ FMQ) plus their relicts, blues symbols secondary spinel compositions that formed by reaction with SiC, red symbols reduced spinels that reacted with silicate melt.

Figure 7. The reduced side of the C-H-O phase diagram. Grey circles denote graphite-saturated C-H-O fluid compositions synthesised by Matveev et al. (1997) at 1273K and 2.4 GPa. Species of fluids along the C saturation line are $CH_4$, $H_2O$, $H_2$, and minor $C_2H_6$. Molar H-O ratios are indicated by contours. Oxygen buffer assemblages (red dots) along the C saturation line are SiC-$SiO_2$-C (SiC, H/O ~ 1000), Fe-FeO (IW, H/O ~ 30), WC-$WO_2$-C (WCO, H/O ~ 14), and Co-CoO (CoO, H/O ~ 4.3). Increasing temperature increases C solubility and shifts the $H_2O$ maximum (inset) to higher C content (Taylor and Green, 1989). Increasing pressure has the opposite effect.

Figure 8. Pressure-volume relations of a $CH_4$-$H_2$ (94/6) fluid in redox equilibrium with SiC at 1600K, calculated with an MRK equation of state (Anderson and Crerar, 1993).

This is the peer-reviewed, final accepted version for American Mineralogist, published by the Mineralogical Society of America.
The published version is subject to change. Cite as Authors (Year) Title. American Mineralogist, in press.
DOI: https://doi.org/10.2138/am-2021-7612. http://www.minsocam.org/


Table 1. Starting materials and experimental phase compositions of three experimental runs at 1600K and 0.7 GPa, with run times ranging from 30 min (cr-9), 2 hrs (cr-6), and 4 hrs (cr-8). $Fe_2O_3$ and CrO where listed were calculated assuming stoichiometry. Cr# = atomic Cr/(Cr + Al + $Fe^{3+}$), Mg# = atomic Mg/(Mg + $Fe^{2+}$), - not detected, n.c. not calculated.

| | Starting materials | | | Experimental compositions, 1600K, 0.7 GPa | | | | | | | |
|---|---|---|---|---|---|---|---|---|---|---|---|
| | oxidised | | | reduced | | | | | | | |
| | olivine | opx | chromite | olivine | olivine | olivine | opx | spinel | spinel | spinel | spinel |
| Oxide | 1 | 2 | 3 | 4 | 5 | 6 | 7 | 8 | 9 | 10 | 11 |
| $SiO_2$ | 40.9 | 55.7 | 0.14 | 41.7 | 42.1 | 42.3 | 52.6 | - | - | 0.14 | 0.11 |
| $TiO_2$ | - | 0.12 | 0.59 | 0.04 | 0.01 | 0.03 | 0.37 | 0.50 | 0.74 | 0.21 | 0.27 |
| $Al_2O_3$ | 0.05 | 1.60 | 15.4 | 0.2 | 0.09 | 0.09 | 4.2 | 14.5 | 17.2 | 53.5 | 56.6 |
| $Cr_2O_3$ | 0.2 | 0.8 | 47.7 | - | - | - | - | 59.8 | 51.5 | 12.1 | 13.5 |
| $Fe_2O_3$ | - | - | 6.20 | - | - | - | - | n.c. | n.c. | n.c. | n.c. |
| CrO | - | - | - | 1.8 | 3.5 | 3.6 | 2.2 | n.c. | n.c. | n.c. | n.c. |
| FeO | 10.7 | 6.1 | 16.6 | 3.03 | 2.49 | 2.4 | 2.47 | 3.20 | 8.10 | 11.8 | 6.12 |
| NiO | 0.3 | n.a. | n.a. | - | - | - | - | - | - | - | - |
| MgO | 48.2 | 32.2 | 11.8 | 53.5 | 52.4 | 52.5 | 35.4 | 20.2 | 22 | 21 | 22.7 |
| CaO | 0.15 | 2.64 | - | 0.23 | 0.19 | 0.19 | 2.16 | - | - | - | - |
| Total | 100.5 | 99.2 | 98.4 | 100.4 | 100.9 | 101.1 | 99.4 | 98.2 | 99.8 | 98.8 | 99.2 |
| cations | 3.00 | 4.00 | 3.00 | 3.00 | 3.00 | 2.99 | 4.00 | 3.00 | 3.06 | 3.03 | 3.00 |
| Mg# | 0.89 | 0.90 | 0.56 | 0.97 | 0.97 | 0.98 | 0.96 | 0.92 | 0.83 | 0.76 | 0.87 |
| Cr# | - | - | 0.62 | - | - | - | - | 0.74 | 0.67 | 0.13 | 0.14 |
| relat. $fO_2$ | --------- FMQ ------- | | | ---------- ~ IW-3 ---------- | | | | | | | |

This is the peer-reviewed, final accepted version for American Mineralogist, published by the Mineralogical Society of America.
The published version is subject to change. Cite as Authors (Year) Title. American Mineralogist, in press.
DOI: https://doi.org/10.2138/am-2021-7612. http://www.minsocam.org/

| | Starting materials | | | Experimental compositions, 1600K, 0.7 GPa | | | | | | | |
|---|---|---|---|---|---|---|---|---|---|---|---|
| | oxidised | | | reduced | | | | | | | |
| | olivine | opx | chromite | olivine | olivine | olivine | opx | spinel | spinel | spinel | spinel |
| Oxide | 1 | 2 | 3 | 4 | 5 | 6 | 7 | 8 | 9 | 10 | 11 |
| $SiO_2$ | 40.9 | 55.7 | 0.14 | 41.7 | 42.1 | 42.3 | 52.6 | - | - | 0.14 | 0.11 |
| $TiO_2$ | - | 0.12 | 0.59 | 0.04 | 0.01 | 0.03 | 0.37 | 0.50 | 0.74 | 0.21 | 0.27 |
| $Al_2O_3$ | 0.05 | 1.60 | 15.4 | 0.2 | 0.09 | 0.09 | 4.2 | 14.5 | 17.2 | 53.5 | 56.6 |
| $Cr_2O_3$ | 0.2 | 0.8 | 47.7 | - | - | - | - | 59.8 | 51.5 | 12.1 | 13.5 |
| $Fe_2O_3$ | - | - | 6.20 | - | - | - | - | n.c. | n.c. | n.c. | n.c. |
| CrO | - | - | - | 1.8 | 3.5 | 3.6 | 2.2 | n.c. | n.c. | n.c. | n.c. |
| FeO | 10.7 | 6.1 | 16.6 | 3.03 | 2.49 | 2.4 | 2.47 | 3.20 | 8.10 | 11.8 | 6.12 |
| NiO | 0.3 | n.a. | n.a. | - | - | - | - | - | - | - | - |
| MgO | 48.2 | 32.2 | 11.8 | 53.5 | 52.4 | 52.5 | 35.4 | 20.2 | 22 | 21 | 22.7 |
| CaO | 0.15 | 2.64 | - | 0.23 | 0.19 | 0.19 | 2.16 | - | - | - | - |
| Total | #### | 99.2 | 98.4 | 100.4 | 100.9 | 101.1 | 99.4 | 98.2 | 99.8 | 98.8 | 99.2 |
| cations | 3.00 | 4.00 | 3.00 | 3.00 | 3.00 | 2.99 | 4.00 | 3.00 | 3.06 | 3.03 | 3.00 |
| Mg# | 0.89 | 0.90 | 0.56 | 0.97 | 0.97 | 0.98 | 0.96 | 0.92 | 0.83 | 0.76 | 0.87 |
| Cr# | - | - | 0.62 | - | - | - | - | 0.74 | 0.67 | 0.13 | 0.14 |
| relat. $fO_2$ | --------- | FMQ | ------- | ---------- | | | | ~ IW-3 | | | |

This is the peer-reviewed, final accepted version for American Mineralogist, published by the Mineralogical Society of America.
The published version is subject to change. Cite as Authors (Year) Title. American Mineralogist, in press.
DOI: https://doi.org/10.2138/am-2021-7612. http://www.minsocam.org/


revision 1

# Ultra-reduced phases in ophiolites cannot come from Earth's mantle

Chris Ballhaus[1]*, Hassan M. Helmy[1], Rául O.C. Fonseca[2], Richard Wirth[3], Anja Schreiber[3], Niels Jöns[2]

[1]Geoscience Institute, University of Bonn, Germany

[2]Institute for Geology, Mineralogy and Geophysics, Ruhr-University of Bochum, Germany

[3]Helmholtz Centre Potsdam, GFZ German Research Centre for Geosciences, Potsdam, Germany

* corresponding author (email: ballhaus@uni-bonn.de)

Key words: ultra-reduced minerals, moissanite, ultra-reduced mantle, ophiolites, oxidation state

## ABSTRACT

A number of recent papers have purported to find ultra-reduced minerals - as natural examples - within ophiolitic mantle sections, including SiC moissanite, Fe-Si alloys, various metal carbides, nitrides, and borides. All those phases were interpreted to be mantle derived. The phases are recovered from mineral concentrates and are assigned to the deep mantle because microdiamonds and other ultra-high pressure (UHP) minerals are also found. Based on these findings it is claimed that the mantle rocks of ophiolite complexes are rooted in the Transition Zone (TZ) or even in the Lower Mantle, at redox states so reduced that phases like SiC moissanite are stable.

We challenge this view. We report high temperature experiments carried out to define the conditions under which SiC can be stable in Earth's mantle. Mineral separates from a fertile lherzolite xenolith of the Eifel and chromite from the LG-1 seam of the Bushveld complex were reacted with SiC at 1600K and 0.7 GPa. At high temperature a redox gradient is quickly established between the silicate/oxide assemblage and SiC, of ~ 12 log-bar units in $fO_2$.

Reactions taking place in this redox gradient allow to derive a model composition of an ultra-reduced mantle by extrapolating phase compositions to 8 log units below the iron-wüstite equlibrium (IW-8) where SiC should be stable. At IW-8 silicate and oxide phases would be pure MgO endmembers. Mantle lithologies at IW-8 would be Fe° metal saturated, would be significantly enriched in $SiO_2$, and all transition elements with the slightest siderophile affinities would be dissolved in a metal phase. Except for the redox-insensitive $MgAl_2O_4$ endmember, spinel would be unstable. Relative to an oxidized mantle at the fayalite-magnetite-quartz (FMQ) buffer, an ultra-reduced mantle would be enriched in enstatite by factor 1.5 since the reduction of the fayalite and ferrosilite components releases $SiO_2$. That mantle composition is unlike any natural mantle lithology ever reported in the literature. Phases as reduced as SiC or Fe-Si alloys are unstable in an FeO bearing hot convecting mantle. Based on our results we advise against questioning existing models of ophiolite genesis because of accessory diamonds and ultra-reduced phases of doubtful origin.

## INTRODUCTION

Until recently it was thought that ophiolites form by spreading of oceanic lithosphere at shallow (~ 50 km) depth (Nicholas, 1999; Pearce and Robinson,

2010; Dilek and Furnes, 2014), most commonly above intra-oceanic subduction zones (Miyashiro, 1973; Robertson 2002). The discovery of UHP minerals in ophiolites worldwide (Robinson et al., 2004; Yang et al. 2015) challenges that view. New models now propose that the mantle lithologies of ophiolites are rooted in the transition zone (TZ) or even in the lower mantle (Griffin et al., 2016a). Some authors even claim that the characteristic ores of supra-subduction zone ophiolites - podiform chromite mineralisations - are enriched at TZ pressure when chromite is in the post-spinel stability field (Xiong et al., 2015).

But how credible are those models? Do microdiamonds in ophiolite lithologies justify rewriting the entire history of ophiolite genesis? The problem is that ophiolitic diamonds are found almost exclusively in heavy mineral concentrates of harzburgite and chromitite bulk samples up to 1000 kilos in size (Robinson et al., 2004; Xu et al., 2015; Yang et al., 2015). The risk of contamination during sample processing is high. Except for three dubioius examples (Yang et al., 2007; 2015; Das et al., 2017) - two of the in-situ diamonds occur in carbon glass - no cases are reported where diamonds were found intergrown with mantle minerals.

In addition to diamonds, the mineral separates return ultra-reduced minerals including SiC, Fe-Si alloys, metal nitrides, carbides, and borides (Fig. 1). These phases also pose a problem. Ophiolites are lithologies that crystallize at oxygen fugacities ($fO_2$) around FMQ. Silicon carbide and Fe-Si alloys, by contrast, afford $fO_2$ conditions of ~ IW-8 (Barin, 1995). At this relative $fO_2$ mantle silicates should be FeO-free, should coexist with (Fe,Ni) metal, and $Cr_2O_3$ in chromite would be reduced to metallic Cr (Schmidt et al., 2014; Golubkova et al., 2016). No such signatures have ever been reported from mantle lithologies.

The diamonds are not the topic of this paper even though their relation to ophiolite lithologies is far from being understood: many "ophiolitic" diamonds carry Mn-Ni-

Co metal inclusions (Yang et al., 2014; 2015; Griffin et al., 2016a), a composition that is used in China as solvent-catalyst to flux industrial diamond synthesis (Sund and Tai, 1997; Zhou et al. 2009; Tan, 2014); those "ophiolitic" diamonds that were analysed for their nitrogen aggregation states are 1B diamonds (Howell et al., 2015; Xu et al., 2017), not exactly a signature consistent with long residence times in the deep mantle; and where "diamondiferous" ultramafic rocks of ophiolite sequences are associated with gabbroic cumulates the latter lack evidence for an UHP overprint (Ballhaus et al., 2018a). We focus here on the ultra-reduced phases (Fig. 1). We report reaction experiments in redox gradients in which mantle silicates and chromite are reacted with SiC. The experiments are intended to clarify (1) if an SiC grain can be stable at ambient mantle temperature and redox state, (2) for how long it would survive the uplift from deeper mantle levels, and (3) what textural and compositional changes a mantle would undergo when it is are exposed to ultra-reduced conditions. The last point allows to identify compositional fingerprints of ultra-reduction, should such fingerprints ever be found in Earth mantle lithologies.

## METHODS

Starting materials for the redox experiments were 65 wt.% lherzolitic materal from a fertile xenolith from Dreiser Weiher (Eifel), 25 wt.% metallurgical-grade chromite from the LG-1 layer of the Bushveld Complex, and ~ 10 wt.% industrial hexagonal SiC. Silicate and oxide phases had grain sizes around 100 µm. Silicon carbide was added in two grain sizes; ~ 1 to 10 µm for the run cr-6 (2 hrs), and as angular grains 100 ± 50 µm in size for the runs cr-8 (4 hrs) and cr-9 (30 min). Aliquots of the materials were loaded in 4 mm outer diameter graphite capsules, then reacted in a piston-cylinder press at 1600K and 0.7 GPa. The pressure

transmitting media were talc-pyrex sleeves. The heating elements were 5 mm inner diameter graphite rods machined from high resistance graphite. To avoid short circuiting, the graphite capsules were shielded from the heaters by 0.5 mm thick boron nitride sleeves. Temperature was controlled with W-Re thermocouples to within ± 20K. Quenching occurred by turning off power supply.

At the beginning of a run when the target temperature of 1600K was approached, a redox gradient of ~ 12 log-bar units developed inside the capsules between the mantle material, chromite, and SiC (Fig. 2). The mantle minerals plus chromite define an $fO_2$ at FMQ (Ballhaus et al., 1991) while SiC imposes at 1600K an upper $fO_2$ limit at ca. IW-8 (Barin, 1995). Thermodynamic equilibrium was not reached but this was not intended. Tje aim instead was to document reactions along a redox gradient, in order to quantify if and for how long ultra-reduced phases like SiC may survive in oxidized (± FMQ) mantle.

Phases were analysed and imaged with a Cameca SX FIVE FE microprobe at the Ruhr University Bochum using natural and synthetic materials as standards (Table 1). Selected textures were imaged at high high resolution with a Zeiss Gemini Sigma 300 VP FE Scanning Electron Microscope (SEM) at the University of Cologne. Many reaction products were too fine-grained to be resolved and quantified by electron probe micro-analysis (EPMA) or SEM. Therefore, four Focussed Ion Beam (FIB) foils were cut (Wirth 2009) from one polished section of the run cr-6 and investigated for reaction textures with a FEI F20 X-Twin Transmission Electron Microscope (TEM) at the GFZ in Potsdam.

## RESULTS

This is the peer-reviewed, final accepted version for American Mineralogist, published by the Mineralogical Society of America.
The published version is subject to change. Cite as Authors (Year) Title. American Mineralogist, in press.
DOI: https://doi.org/10.2138/am-2021-7612. http://www.minsocam.org/


In Figure 3 we summarise backscattered electron (BSE) images and element distributions of relevant phases and textures. Phases identified are two (relict and product) generations of olivine and orthopyroxene, one generation of clinopyroxene, and three generations of spinel. Minor phases are (Fe,Ni), (Fe,Cr), and Fe-Cr-Si metal alloys, relict SiC, metallic Si, and silicate glass pools. Figure 4 documents element distributions to illustrate qualitative compositional changes with progressive reduction. Many reactions are only discernible on the nanoscale, and for that reason we display in Figure 5 TEM images that document phases not resolvable by EPMA. The positions of the FIB foils are marked on Figure 3A and G.

*Silicates*

Olivine of the starting material (analysis 1) reacted with SiC either by forming localised reaction rims (Fig. 3A) or by whole-sale reduction (Fig. 3B to D). The reduction reaction is

$$(Fe,Ni)_2SiO_4 \text{ (in olivine)} + SiC = 2(Fe,Ni)^\circ \text{ (metal)} + 2SiO_2 + C \text{ (graphite capsule)} \quad (1)$$

Product phases are a second generation of olivine, Ni-free within EPMA detection limit (~ 200 ppm) but significantly more magnesian than olivine of the starting mix (analyses 4 to 6). On the nanoscale, product olivine is peppered with an α-(Fe,Ni) metal phase (Fig. 5A). The most forsteritic, post-reduction olivine composition analysed was $Fo_{98}$ but given the sizes and abundances of nanoscale α-(Fe,Ni) inclusions there is no guarantee that $Fo_{98}$ indeed is the most magnesian composition.

Relative to the primary starting olivine, reduced olivines are enriched in Cr to up to 3.6 in Cr oxide (analyses 4 to 6). This concentration seems excessive but several analyses on different grains confirmed this to be the case. Normally, mantle olivine at around FMQ carries Cr as a trace constituent (analysis 1) and Cr is trivalent (Li et al., 1995). In highly reduced Moon basalts (Haggerty, 1978) olivine phenocrysts do contain Cr in the percentage range, and Cr is at least in part divalent (Schreiber, 1979; Sutton et al., 1993; Li et al., 1995) but not as Cr enriched as here. We have calculated here Cr in the reaction olivines tentatively as a CrO component (Table 1) to satisfy the cation-oxygen (3:4) ratio of olivine (Table 1).

Reaction (1) sets free $SiO_2$ both by reduction of fayalite to metallic Fe and by the oxidation of SiC to $SiO_2$. We expected that inside the reduction rims (Fig. 3A) orthopyroxene rather than olivine would be stable but that phase was not identified in the rims. We do note both relict and product orthopyroxene outside the reduction rims in the groundmass (analyses 2 and 7), the latter usually as microcrysts in glass (former melt) pools. Reduced orthopyroxene is nearly as magnesian as reduced olivine ($En_{96}$) and quite enriched in Cr. To satisfy cation-oxygen stoichiometry constraints we calculated Cr as CrO (analysis 7).

*Oxides*

Chromite also reacted with SiC (Fig. 3E to G). It was surprising to note how quickly and easily a phase as refractory as LG-1 chromite disintegrated upon exposure to SiC (IW-8). The original Bushveld chromite (analysis 3 in Table 1) decomposed to inclusion-rich grain aggregates with several generations of spinel (analyses 8 to 11) highly variable in their Cr/Al and Mg/(Mg+Fe) atomic ratios. In BSE images (Fig. 3E to G) and in the element maps (Fig. 4) secondary spinels are

easily recognised by their lower atomic number contrasts and by ultra-fine < 1 μm wide (Fe,Cr)° metal veinlets. On the nanoscale, reduced spinels are peppered with euhedral (Fe,Cr) metal inclusions up to 200 nm in size (Fig. 5B,C). One FIB foil through a secondary spinel returned, in addtition, ferroan periclase inclusions. We assume that this phase is an excess product left over after FeO, $Fe_2O_3$, and $Cr_2O_3$ were reduced to metal components.

We identify three generations of spinel (Fig. 6): relicts of LG-1 chromite (in black); a compositional array (in red) trending with progressive reduction toward slightly elevated Cr# and much increased Mg# and corresponding to the low atomic contrast spinel rims around LG-1 relicts visible in Fig. 3E, F, and H; and a spinel generation markedly enriched in Al component (in red). This generation is noted near silicate melt (now glass) pools (Fig. 3G) and seems to have exchanged Cr and Al by reaction with melt.

We note that some secondary spinels have slight cation excesses when their stoichiometries are calculated to 4 oxygens. Normally, one would then calculate some FeO as magnetite component, however, for spinels that carry (Fe,Cr) metal inclusions this would seem unintuitive. The bright field image in Fig. 5D indicates that reduced spinels are defect-rich, hence may not be stoichiometric. Chromium in spinel was calculated throughout as an $MCr_2O_4$ ($Cr^{3+}$) component (Table 1) even though at 1600K and the relative $fO_2$ (see below) much of the bulk Cr may have been divalent (Li et al., 1995; Berry and O'Neill 2004). Stubican and Greskovich (1975) presented experiments to show that owing to its high octahedral field stabilisation energy the $Cr^{3+}$ cation is strongly fractionated by spinel but $Cr^{2+}$ in spinel does occur.

*Reduced phases*

In the 2-hour run cr-6 SiC does not seem to have survived. Silicon carbide was added to this run rather fine-grained to promote rapid reduction. In the two other runs with 100±50 µm grain sizes SiC did survive (Fig. 3I) although local oxidation is evident. After only 30 min at 1600K relict SiC grains are surrounded by up to 5 µm wide reaction rims. The rims (Fig. 3J) carry nano-sized $SiO_2$ phases (? tridymite), are highly porous, and are reminiscent of solution-precipitation textures documented by Putnis (2002). Additional ultra-reduced phases include rare metallic Si, likely to be an impurity in the industrial-grade SiC starting material, plus heterogeneous (Fe,Ni,Cr,Si) metal phases: Ni enriched near olivine, Cr enriched when the metal is intergrown with spinel, and Si enriched near relict SiC grains. Larger metals can be exsolved (Fig. 3K), notably those enriched in Si. One single grain of metallic Cr was found (bright spot in Fig. 3K) but that grain must be metastable. In a bulk system with excess molar FeO over $Cr_2O_3$ and metallic Fe, metallic Cr should dissolve in the Fe metal phase.

*Oxygen fugacity prior to quenching*

The coexistence of olivine ($Fo_{98}$) with (Fe,Ni) metal permits to approximate the relative $fO_2$ prior to quenching using the equilibrium $Fe_2SiO_4 = 2Fe + SiO_2 + O_2$ and $\log fO_2 = \Delta G_{r,T} / (2.3 * R * T) + \log a_{Fa}^{ol} - 2 \log a_{Fe}^{metal} - \log a_{SiO2}^{glass}$. Olivine solid solutions are symmetric with a Margules parameter around 3 kJ $mol^{-1}$ (Wiser and Wood, 1991; O'Neill et al., 2003) but given the low fayalite content ($X_{Fa}^{ol} = 0.02$) and a run temperature of 1600K we suggest that $a_{Fa}^{olivine} = X_{Fa}^{2}$ is considered sufficiently precise. For iron in the (Fe,Ni) metal phase we ignore the Ni content (around 1 wt.% with local variations) and set $a_{Fe}^{metal}$ at unity. The $SiO_2$ activity is

approximated from the average mole fraction of $SiO_2$ in orthopyroxene saturated silicate glasses to 0.4. It follows that the $fO_2$ gradient, initially ~ 12 log-bar units, must have converged with run time to around IW-3 to IW-3.5 (Fig. 2). No fundamental differences are noted among the runs or with run time.

## DISCUSSION

It is clear from the results that at best local (grain-scale) redox equilibrium was achieved. We found relict and product olivine and orthopyroxene. We identified a range of spinel compositions that would have been homogenized to one phase had the runs not been quenched before global (capsule-scale) equilibrium was reached. The Cr, Ni, and Si concentrations in Fe metal are variable and controlled by local-scale environments. We identified three Cr oxidation states if the allocations of Cr to olivine (divalent), spinel (trivalent), and metal phases (zero) in Table 1 are correct. Note though that multiple Cr oxidation states are not necessarily indicative of disequilibrium (cf. Rohrbach et al., 2007). At IW-3 and 1600K three Cr oxidation states may have coexisted even though $Cr^{2+}$ should have been by far the prevalent species (Berry and O'Neill, 2004). Each Cr-bearing phase would then fractionate the Cr species that is most easily accommodated in its lattice.

### *The mantle at IW-8*

We may extrapolate the redox reactions to IW-8 and derive a model mantle composition that would be stable with SiC. Silicates would be reduced to their MgO endmembers, and their FeO and NiO components would be precipitated as (Fe,Ni) metal phase (cf. O'Neill and Wall, 1987). Reduction of fayalite and ferrosilite liberates $SiO_2$ (eqn. 1), hence modal orthopyroxene would increase. That

increase would not be insignificant: a harzburgite at FMQ with 80% $Fo_{92}$ and 20% $En_{92}$ reduced to IW-8 would liberate by fayalite and ferrosilite reduction 0.8 * 8 plus 2 * 0.2 * 8 moles of $SiO_2$ respectively, in total 9.6 moles $SiO_2$. A harzburgite in equilibrium with SiC would then be composed of ca. 70% forsterite and 30% enstatite plus a few percent metallic (Fe,Ni,Cr) alloys, compared to 80:20 (ol:opx) in a metal free harzburgite at FMQ.

At IW-8, spinel would have a small stability field. We do note that with progressive reduction Cr is enriched in spinel (cf. blue array in Fig. 6), however, our experiments were greatly enriched in chromite and no capsule-scale redox equilibrium was reached. In a reduced natural harzburgite at SiC the Cr, Ni, and Fe components would be reduced to (Fe,Cr) metal, and all transition elements with the slightest siderophile affinity would be dissolved in the Fe metal phase. The only spinel composition insensitive to reduction is $MgAl_2O_4$ but that endmember has a small stability field (Klemme and O'Neill, 2000). Above ca. 2 GPa, an ultra-reduced mantle composition would probably be garnet $(Mg,Ca)_3Al_2Si_3O_{12}$ saturated.

We do find mantle lithologies in Archaean cratonic lithosphere with vaguely similar signatures (Kelemen et al., 1992) but they are not metal saturated. Perhaps they were in the distant past?

*Ultra-reduced minerals - stable in upper mantle lithologies?*

Ultra-reduced phases like SiC or Fe-Si alloys or Ti carbides in ophiolites are highly unstable in Earth's mantle. Silicon carbide becomes oxidised quickly by reducing the FeO, NiO, and $Cr_2O_3$ components of mantle minerals to (Fe,Ni,Cr)° metal and divalent Cr. Reaction rates at 1600K (ambient asthenospheric temperature) are

rather fast, given that after only 30 min at 1600K SiC fragments are rimmed by up to 5 μm wide $SiO_2$ reaction rims (Fig. 3J). It is speculative to connect experimental reaction rates with mantle uplift rates, but we infer that convecting upper mantle at 400 km depths (cf. Xiong et al., 2015) would have to be exhumed within months to years to retain SiC grains 100 μm in size, much faster than uplift rates brought into discussion by Griffin et al. (2016a). Pressure has no significant effect. Even though our experiments were carried out at relatively low pressure (0.7 GPa) the $fO_2$ gradient of 12 log units (Fig. 2) can be safely extrapolated to the deeper mantle (Ulmer et al., 1998; Golubkova et al., 2016). Single oxygen buffers do have pressure terms but when the differences between two solid-state buffers are computed individual pressure effects largely cancel out.

*Ultra-reduced phases - textural and chemical considerations*

The ultra-reduced phases are unstable also on textural grounds. We illustrate this fact with characteristic textures illustrated in Figure 1.

Intra-grain exsolutions (Fig. 1A), symplectitic textures (Fig. 1B,C), and skeletal crystal morphologies (Fig. 1D-F) have rather unfavourable surface to volume ratios, and texturally they are highly unstable. Skeletal crystals typically grow in large temperature and/or chemical potential gradients when the rate of diffusion is slow relative to the cooling rate (Bryan, 1972; Donaldson, 1976). Such conditions are hard to reconcile for the asthenosphere. In a hot convecting mantle regime all those textures would recrystallise spontaneously to equant grains, in an effort to minimise their surface energies. They would not form in hot asthenosphere with no local (grain-scale) gradients, and even if they did form by some miraculous process

they would have no chance to survive uplift to Earth's surface for any length of time.

A rather critical case are the SiC grains in Figure 1G, one of the finds termed *"in-situ"* because SiC is enclosed by chromite. Liang et al. (2014) who illustrated this example did not characterise the dark (low atomic contrast) matrix around the SiC fragments, so it is unclear if SiC occurs in a void or a light element matrix like carbon (cf. Yang et al., 2007). Nor did they document that the composition of the spinel in contact with SiC reacted locally to the low redox state imposed by SiC. Angular SiC fragments, potentially in voids, are not what we expect from *"in-situ"* SiC inclusions that were trapped at high pressure under convecting mantle conditions. That the angular SiC grains are UHP phases as asserted can only be entertained if the host chromite is proven to have crystallised initially in the orthorhombic calcium ferrite (CF) structure (Chen et al., 2003). Liang et al. (2014) failed to demonstrate this.

Many other phases considered to be mantle derived also raise issues. For example, Yang et al. (2015) recovered from the Ray Iz ophiolite ultra-reduced phase populations including metallic Zr, Ta, Ta-Co alloys, metallic Cr, and tungsten carbide aggregates. At 1600K metallic Zr is around 7 orders more reduced than SiC (Barin, 1995), so would we now allocate the Ray Iz ophiolite a relative $fO_2$ of IW-15? As for metallic Ta, there is no natural process known that would separate the geochemical twins Nb and Ta to the extent that pure Ta metal results. The Nb-Ta ratio of Earth's mantle is ~ 14 (Münker et al., 2003; Witt-Eickschen and O'Neill, 2005), hence large quantities of Nb would have to "disappear" before pure Ta could form. The phase more stable would be metallic Nb, not Ta, since Nb is more siderophile than Ta (Wade and Wood, 2001). The WC aggregates in Figure 1H and 1I are also dubious. The matrix to the euhedral WC grains appears to be metallic

Co, a metal that is used industrially to sinter WC crystals to carbide metal. We find it disturbing to note that both WC images are identical (i.e. from the same aggregate), yet that they were reported as having been derived from two ophiolites more than 4600 km apart: Figure 1H from Ray Iz in the Polar Urals (Yang et al., 2015), Figure 1I from Luobusa in Tibet (Fang et al., 2009).

The ferroan ringwoodite (Rw) skeletons in Figure 1J, now named ahrensite, from a siliceous pumice in Spain (Díaz-Martinez and Ormö, 2003; Glazovskaya and Feldman, 2010) are not reduced. We do include them nonetheless in our compilation to illustrate that UHP phases may also nucleate metastably outside their stability fields; as do coesite (Bouška and Feldman, 1994), stishovite (Shveikin et al., 2015), and diamond (Angus and Hayman, 1988; Farré-de-Pablo et al., 2018). Before one speculates on UHP histories of ophiolites, one should document the crystal shapes of the UHP phases to help judge the reader if they could be metastable in origin.

*Can ultra-reduced phases be stabilised by $CH_4$-$H_2$ fluids?*

Griffin et al. (2016b; 2019; 2020), Xiong et al. (2017), and Bindi et al. (2019) documented skeletal corundum-hibonite-grossite fragments from the Kishon River at the foothills of the Mt. Carmel basaltic complex, northern Israel. The aggregates carry ultra-reduced phases like TiN osbornite, $Ti_2O_3$ tistarite, V metal, (V,Al) alloys, and V hydrides (Fig. 1E,F). Although the fragments have nothing to do with ophiolites, they do fit in this paper because the mode proposed of their origin - infiltration of the mantle sources by ultra-reduced $CH_4$-$H_2$ fluids - was recently applied to stabilise ultra-reduced phases in ophiolites as well (Xiong et al., 2017).

We test by mass balance how much $CH_4$-$H_2$ fluid would have to be infiltrated in a mantle source to reduce all FeO and stabilise SiC. As infiltration fluid we choose a C-H-O composition in equilibrium with SiC synthesised by Matveev et al. (1997). These authors combusted organic C-H-O compounds to C-H-O fluids at 1273K and 2 GPa in the presence of solid state oxygen buffers, including SiC-$SiO_2$-C (Fig. 7). Fluids in equilibrium with SiC and graphite were analysed by gas chromatography and mass spectrometry and had 91.4 ± 0.5 mole% $CH_4$, 1.9 ± 0.1 mole% $C_2H_6$, 6 ± 0.4 mole% $H_2$ with traces of $H_2O$ at the detection limit. The molar H-O ratio was 900 ± 550 (n = 3).

As for the mantle material, we choose a mantle composition with 8 wt.% FeO (Palme and O'Neill, 2014). One cubic meter of that material contains 3900 moles FeO. The bulk reduction reaction with the SiC fluid composition specified above would then be

$$1.94\ FeO + 0.06\ H_2 + 0.94\ CH_4 = 1.94\ Fe° + 1.94\ H_2O + 0.94\ C \qquad (2)$$

To simplify things we allot $C_2H_6$ to $CH_4$. To reduce 3900 moles FeO to Fe° ca. 2000 moles of $CH_4$-$H_2$ (94/6) fluid must be infiltrated. We follow Griffin et al. (2019) and assume the fluid was infiltrated at 0.7 GPa near the MOHO. We set the infiltration temperature to 1600K appropriate for a time of intense magmatic activity at Mt. Carmel. At these P-T conditions the volume of 2000 moles $CH_4$-$H_2$ (94/6) fluid is approximated with an MRK EoS (Anderson and Crerar, 1993) to ~ 0.1 $m^3$. The molar volume is around 48 $cm^3$.

A fluid-rock volume ratio of 0.1 seems reasonable but note that the infiltration depth (near the MOHO) is an *ad hoc* estimate by Griffin et al. (2019) unconstrained by independent evidence. Had the hypothetical fluid been infiltrated at shallower depth the fluid-rock ratio would increase dramatically with falling

This is the peer-reviewed, final accepted version for American Mineralogist, published by the Mineralogical Society of America.
The published version is subject to change. Cite as Authors (Year) Title. American Mineralogist, in press.
DOI: https://doi.org/10.2138/am-2021-7612. http://www.minsocam.org/


pressure and would soon become unrealistic (Fig. 8). More important, however, are the following concerns:

- How was it possible that the mantle that produced basalts with 12 wt.% FeO + $Fe_2O_3$ (Kaminchik et al., 2014) emanated ultra-reduced $CH_4$-$H_2$ fluids? Alkali basalts are oxidized around FMQ+1 and their equilibrium volatiles are $H_2O$ and $CO_2$. Griffin et al. (2020) realised that problem but circumvented it by stating (rather *ad hoc*) the fluid infiltration episode was unrelated to the alkali basaltic volcanism. No reasons are given for that assertion.

- Corundum (Fig. 1F) and $(Al,Cr)_2O_3$ solid solutions afford temperatures in excess of 2270K (Muan and Somiya, 1959). Phases in the system $Al_2O_3$-$Ti_2O_3$-$TiO_2$ including tistarite $Ti_2O_3$ crystallise at around 1900K (Jung et al., 2009). Hibonite-grossite-corundum assemblages record minimum temperatures around 1875K if they once coexisted with melt (cf. Jerebtsov and Mikhailov, 2001). Metallic V reported by Bindi et al. (2019) has a liquidus temperature of 2180K (Murray 1989). Temperatures in that range are unrealistic for a Cretaceous volcanic province. The MgO contents of primitive Mt. Carmel basalts (Kaminchik et al., 2014), around 13 to 14 wt.% plus perhaps 0.5 wt.% $H_2O$ + $CO_2$, constrain the liquidus temperature to around 1520K (Helz and Thornber, 1987).

- When sapphire crystals are entrained as xenocrysts in alkali basalts they react to spinel via $Al_2O_3 + (MgO,FeO)_{basalt} = (Mg,Fe)Al_2O_4$. The reaction is fast (Baldwin et al., 2017). So why are the corundum fragments not mantled by spinel coronas if they were carried to the surface by FeO rich hot alkali basalts, for a distance of 25 to 30 km?

- Why should corundum-hibonite-grossite-tistarite aggregates be skleletal (Fig. 1F and Xiong et al., 2017) if they crystallised from natural basalts or their mantle sources at depth?

- Griffin et al. (2020) believe they identified relicts of the reducing fluid. They assert that voids in their Mt. Carmel fragments were filled originally by $H_2$ - a rather adventurous proposition when by definition a void is empty.

- The vanadium metal and (V,Al) alloys (Fig. 1E and Griffin et al., 2019) may be small but by what natural process were V oxide components enriched to up to 100 wt.% then reduced to their metal states, when alkali basalts contain ~ 250 to 300 ppm V as oxide component (Doe, 1997) and ca. 15 wt.% $Al_2O_3$? What type of magmatic fractionation process selectively enriched V and Al?

- Why were no ultra-reduced, FeO-free silicates picked up by the alkali basalts of Mt. Carmel if the mantle source was that reduced?

We agree with Litasov et al. (2019) that the skeletal corundum-rich fragments of the Kishon river locality are anthropogenic in origin. They could be relicts/refuse of the aerospace and/or medical implant industry where Ti-Al-V light metal alloys are cast into refractory moulds composed of fused alumina and zirconia and occasionally yttria. After freezing, the metal-contaminated mould is being knocked off and disposed. The metal itself is melted from constituents in the form of pure Ti metal sponge and an Al-V pre-alloy where large chunks are typically subjected to a process of hydridation - dehydridation for easier comminution. Melting and casting of Ti-Al-V alloys take place under vacuum or protective atmosphere since Ti-Al-V alloys are extremely reactive with air. Even in an already frozen hot stage the alloys easily react with $N_2$ to form nitrides (A. Bouvier and K. Rabitsch, pers. comm. 2020).

Hydrogenation and nitridation may stabilise metal hydrides and nitrides - phases that were described by Griffin et al. (2019) and Bindi et al. (2019) and "sold" as minerals. We propose that the Kishon River aggregates are fragments of zirkonia-lined alumina casting moulds that were infiltrated by Ti-Al-V melts. Following Litasov et al. (2018) we rule out a natural origin and a genetic connection to the Cretaceous Mt. Carmel basalts.

## IMPLICATIONS

Ultra-reduced phases such as SiC or Fe-Si alloys would have no chance of forming or surviving for any length of time in FeO bearing asthenospheric mantle. Silicon carbide, arguably the most prominent among the ultra-reduced phases in ophiolites, is unstable both chemically and texturally. Silicon carbide is incompatible with almost every aspect of known mantle mineralogy. Based on a few exotic phases of doubtful provenance it does not seem target-oriented to rewrite the history of ophiolites so fundamentally as proposed by Griffin et al. (2016a) and Xiong et al. (2015).

That diamonds and ultra-reduced phases are found in the same heavy mineral concentrates does not mean a genetic link must exist between these phases and ophiolites. The diamonds could be contamination, notably those with Mn-Ni-Co metal melt inclusions (Yang et al., 2014; 2015; Griffin et al., 2016a), diamonds with trace element signatures identical to Russian and Chinese synthetics (Litasov et al., 2019), and diamonds with (young) 1B nitrogen aggregation states.

Ballhaus et al. (2017) noted that some ultra-reduced phases in ophiolite concentrates resemble minerals in fulgurites. They exposed basalts and ultramafic mantle rocks to electric discharges at 9.9 kV and 30 kA at temperatures in excess

of 6000K simulating temperatures when lightning bolts strike solid rocks. At 6000K lithologies are vaporised to plasmas. The first and highest temperature precipitates of the plasmas were silicon, Fe-Si silicides, SiC, metals, metal alloys, and amorphous carbon, exactly the phases found in ophiolite concentrates. There is no reasonable reason argument that can be made to oppose analogies to fulgurites (cf. Griffin et al., 2018; Yang et al., 2018; Xiong et al., 2019):

- plasmas produce perfectly rounded spherules when they are quenched in air (Genareau et al., 2015), and these spherules are found in both ophiolite concentrates (Yang et al., 2015; Griffin et al., 2016a), in surface sediments of ophiolites (Zuxiang, 1984), and as ejecta of the Ballhaus et al. (2017) experiments;
- plasmas quench extremely rapidly and produce skeletal crystal morphologies as those compiled in Figure 1 (cf. Essene and Fisher, 1986); and
- plasmas solve the redox paradox as they may condense within any lithology on any type of surface, regardless of the redox states of the rocks within which they occur.

Lightning bolts are one hypothesis among others. Diamonds, SiC, and Fe-Si alloys may well form metastably at low temperature and pressure (Angus and Hayman, 1988; Ishimaru et al., 2009; Schmidt et al., 2014; Shiryaev and Gaillard, 2014; Farré-Paolo et al., 2018; Pujol-Solà et al., 2020). In addition, there is a certain probability that many ultra-reduced phases reported from ophiolites and elsewhere simply arise from contamination during sample handling and lack of due diligence by the original authors in looking for possible sources of contamination before ruling it out.

This is the peer-reviewed, final accepted version for American Mineralogist, published by the Mineralogical Society of America.
The published version is subject to change. Cite as Authors (Year) Title. American Mineralogist, in press.
DOI: https://doi.org/10.2138/am-2021-7612. http://www.minsocam.org/


## ACKNOWLEDGEMENTS

We thank the machine shops of the Geoscience Institute for keeping the experimental equipment in excellent running order. Matthias Gottschalk and Jamie Connolly greatly helped in checking the PVT properties calculated for $CH_4$-$H_2$ fluids. Alexander Bouvier and Kurt Rabitsch of the Treibach Industrie AG directed the first author to process technologies used in the production of Ti-Al-V light metal casts. Hanna Cieszynski kindly imaged selected textures with FE-SEM at high resolution. Insightful comments by Hugh O'Neill and an anonymous reviewer, as well as efficient editorial handing by Fabrizio Nestola are greatly appreciated. Funded by the German Science Foundation (DFG) through grant Ba 964/37 to Chris Ballhaus, through a Georg Forster Prize awarded by the Alexander von Humboldt Foundation to Hassan M. Helmy, and through a Heisenberg Professorship to Raúl O.C. Fonseca by the DFG via grant number FO 698/11-1.

## REFERENCES CITED

Anderson, G.M., and Crerar, D.A. (1993) Thermodynamics in Geochemistry. The Equilibrium Model. Oxford University Press, 588 p.

Angus, J.C., and Hayman, C.C. (1988) Low-pressure, metastable growth of diamond and "diamondlike" phases. Science, 241, 913-921.

Baldwin, L.C., Tomaschek, F., Ballhaus, C., Gerdes, A., Fonseca, R.O.C., Wirth, R., Geisler, T., and Nagel, T. (2017) Petrogenesis of alkaline basalt-hosted sapphire megacrysts. Petrological and geochemical investigations of in situ sapphire occurrences from the Siebengebirge Volcanic Field, Germany. Contributions to Mineralogy and Petrology, 172, 43, DOI 10.1007/s00410-017-1362-0.

Ballhaus, C., Berry, R.F., and Green D.H. (1991) Experimental calibration of the olivine-orthopyroxene-spinel oxygen barometer - implications for oxygen fugacity in the Earth's upper mantle. Contributions to Mineralogy and Petrology, 107, 27-40.

Ballhaus, C., Wirth, R., Fonseca, R.O.C., Blanchard, H., Pröll, W., Bragagni, A., Nagel, T., Schreiber, A., Dittrich, S., Thome, V., Hezel, D.C., Below, R., and Cieszynski, H. (2017) Ultra-high pressure and ultra-reduced minerals in ophiolites may form by lightning strikes. Geochemical Perspectives Letters, 5, 42-46.

Ballhaus, C., Fonseca, R.O.C., and Bragagni, A. (2018a) Reply to Comment on “Ultra-high pressure and ultra-reduced minerals in ophiolites may form by lightning strikes” by Griffin et al. (2018): No evidence for transition zone metamorphism in the Luobusa ophiolite. Geochemical Perspectives Letters, 7. doi: 10.7185/geochemlet.1810.

Ballhaus, C., Blanchard, H., Fonseca, R.O.C., and Bragagni, A. (2018b) Reply 2 to comment on “Ultra-high pressure and ultra-reduced minerals in ophiolites may form by lightning strikes". Geochemical Perspectives Letters, 8, 8-10 | doi: 10.7185/geochemlet.1821.

Barin, I. (1995) Thermochemical data of pure substances I + II, 3rd edition. VCH Verlagsgesellschaft, 1885 p.

Berry, A.J., and O'Neill, H.St.C. (2004) A XANES determination of the oxidation state of chromium in silicate glasses. American Mineralogist, 89, 790-798.

Bindi, L., Cámara, F., Griffin, W.L., Huang, J.X, Gain, S.E.M, Toledo, V., and O'Reilly, S.Y. (2019) Discovery of the first natural hydride. American Mineralogist, 104, 611–614.

Bouška, V., and Feldman, V.I. (1994) Terrestrial and lunar, volcanic and impact glasses, tektites, and fulgurites. In Marfunin, A.S. (ed.) Advanced Mineralogy 258-265. doi:10.1007/978-3-642-78523-8.

Bryan, W.B. (1972) Morphology of quench crystals in submarine basalts. Journal of Geophysical Research, 77, 5812-5819.

Chen, M., Shu, J., Mao, H.K., Xie, X., and Hemley, R.J. (2003) Natural occurrence and synthesis of two new postspinel polymorphs of chromite. PNAS, 100, 14651-14654.

Das, S., Basu, A.R., and Mukherjee, B.K. (2017) In situ peridotitic diamond in Indus ophiolite sourced from hydrocarbon fluids in the mantle transition zone. Geology, 45, 755–758.

532 Díaz-Martinez, E., and Ormö, J. (2003) An alternative hypothesis for the origin of
533 ferroan ringwoodite in the pumice of El Gasco (Cáceres, Spain). Lunar and
534 Planetary Science XXXIV, 1318.

535 Dilek, Y., and Furnes, H. (2014) Ophiolites and their origins. Elements, 10, 93–
536 100.

537 Dobrzhinetskaya, L.F., Wirth, R., Yang, J., Hutcheon, I.D., Weber, P.K., and
538 Green II, H.W. (2009) High-pressure highly reduced nitrides and oxides from
539 chromitite of a Tibetan ophiolite. PNAS, 106, 19233-19238.

540 Doe, B.R. (1997) Geochemistry of oceanic igneous rocks — ridges, islands, and
541 arcs — with emphasis on manganese, scandium, and vanadium. International
542 Geological Review, 39, 1053-1112.

543 Donaldson, C.H. (1976) An experimental investigation of olivine morphology.
544 Contributions to Mineralogy and Petrology, 57, 187-213.

545 Essene, E.J., and Fisher, D.C. (1986) Lightning strike fusion: Extreme reduction
546 and metal-silicate liquid immiscibility. Science, 234, 189-193.

547 Fang, Q., Bai, W., Yang, J., Xu, X., Li., G. Shi, N., Xiong, M., and Rong, H.
548 (2009) Qusongite (WC): A new mineral. American Mineralogist, 94, 387-390.

549 Farré-de-Pablo, J., Joaquín, A., Proenza, J.A., González-Jiménez, J.M., Garcia-
550 Casco, A., Colás, V., Roqué-Rossell, J., Camprubí, A., and Sánchez-Navas, A.
551 (2018) A shallow origin for diamonds in ophiolitic chromitites. Geology, 47, 75-
552 78.

553 Gao Z., and Lu H. (2016) Preparation of Ti-Al-V alloys by aluminothermic
554 reaction. In: Li L. et al. (eds) Energy Technology 2016. Springer, Cham.
555 https://doi.org/10.1007/978-3-319-48182-1_8.

Genareau, K., Wardman, J.B., Wilson, T.M., McNutt, S.R., and Izbekov, P. (2015) Lightning-induced volcanic spherules. Geology, 43, 319–322.

Glazovskaya, L.I., and Feldman, V.I. (2010) Petrology of ringwoodite bearing pumices of the El Gasco region, West Spain. European Planetary Science Congress EPSC2010-75 (abstract).

Golubkova, A., Schmidt, M.W., and Connolly, J.A.D. (2016) Ultra-reducing conditions in average mantle peridotites and in podiform chromitites: a thermodynamic model for moissanite (SiC) formation. Contributions to Mineralogy and Petrology, 171, doi: 10.1007/s00410-016-1253-9.

Griffin, W.L., Afonso, J.C., Belousova, E.A., Gain, S.E., Gong, X.-H., González-Jiménez, J.M., Howell, D., Huang, J.-X., McGowan, N., Pearson, N.J., Satsukawa, T., Shi, R., Williams, P., Xiong, Q., Yang, J.-S., Zhang, M., and O'Reilly, S.Y. (2016a) Mantle recycling: Transition zone metamorphism of Tibetan ophiolitic peridotites and its tectonic implications. Journal of Petrology, 57, 655-684.

Griffin, W.L., Gain, S.E.M., Adams, D.T., Huang, J-X., Saunders, M., Toledo, V., Pearson, N.J., and O'Reilly S.Y. (2016b) First terrestrial occurrence of tistarite ($Ti_2O_3$): Ultra-low oxygen fugacity in the upper mantle beneath Mount Carmel, Israel. Geology 44, 815-818.

Griffin, W.L., D. Howell, D., Gonzalez-Jimenez, J.M., Xiong, Q., and O'Reilly, S.Y. (2018) Comment on "Ultra-high pressure and ultra-reduced minerals in ophiolites may form by lightning strikes" by Ballhaus et al. (2017): Ultra-high pressure and super-reduced minerals in ophiolites do not form by lightning strikes. Geochemical Perspectives Letters, 7, 1-2 | doi: 10.7185/geochemlet.1809.

Griffin, W.L., Gain, S.E.M., Huang, J.-X., Saunders, M., Shaw, J., Toledo, V., and O'Reilly, S.Y. (2019) A terrestrial magmatic hibonite-grossite-vanadium

assemblage: Desilication and extreme reduction in a volcanic plumbing system, Mount Carmel, Israel. American Mineralogist, 104, 207–219.

Griffin, W.L., Gain, S.E.M., Cámara, F., Bindi, L., Shaw, J., Alard, O., Saunders, M., Huang, J.-X., Toledo, V., and O'Reilly, S.Y. (2020) Extreme reduction: Mantle-derived oxide xenoliths from a hydrogen-rich environment. Lithos, https://doi.org/10.1016/j.lithos.2020.105404.

Haggerty, S.E. (1978) The redox state of planetary basalts. Geophysical Research Letters, 5, 443-446.

Helz, R.T., and Thornber, C.R. (1987) Geothermometry of Kilauea Iki lava lake, Hawaii. Bulletin Volcanology, 49, 651-66.

Howell, D., Griffin W.L., Yang, S., Gain S., Stern, R.A., Huang, J.-X., Jacob, D.E., Xu, X., Stokes, A.J. O'Reilly, S.Y., and Pearson, N.J. (2015) Diamonds in ophiolites: Contamination or a new diamond growth environment? Earth and Planetary Science Letters, 430, 284–295.

Ishimaru, S., Arai, S., and Shukuno, H. (2009) Metal-saturated peridotite in the mantle wedge inferred from metal-bearing peridotite xenoliths from Avacha volcano, Kamchatka. Earth and Planetary Science Letters, 284, 352–360.

Jerebtsov, D.A., and Mikhailov, G.G. (2001) Phase diagram of $CaO$-$Al_2O_3$ system. Ceramics International, 27, 25-28.

Jung, I.-H., Eriksson, G., Wu, P., and Pelton, A. (2009) Thermodynamic modeling of the $Al_2O_3$–$Ti_2O_3$–$TiO_2$ system and its applications to the Fe–Al–Ti–O inclusion diagram. ISIJ International, 49, 1290–1297.

Kaminchik, J., Segev, A., and Katzir, Y. (2014) The origin of intraplate alkaline mafic magmatism in continental shelves: lavas and xenoliths from the Upper

Cretaceous volcanoes of Mt Carmel. Geological Survey of Israel Publication, 9, 99 p.

Kelemen, P.B., Dick, H.J.B., and Quick, J.E (1992) Formation of harzburgite by pervasive melt/rock reaction in the upper mantle. Nature, 358, 635-641.

Klemme, S., and O'Neill, H.St.C. (2000) The near-solidus transition from garnet lherzolite to spinel lherzolite. Contributions to Mineralogy and Petrology, 138, 237-248.

Li, J.-P., O'Neill, H.St.C, and Seifert, F. (1995). Subsolidus phase relations in the system MgO—$SiO_2$—Cr—O in equilibrium with metallic Cr, and their significance for the petrochemistry of chromium. Journal of Petrology, 36, 107-132.

Liang, F., Xu, Z., and Thao, J. (2014) In-situ moissanite in dunite: deep mantle origin of mantle peridotite in Luobusa ophiolite, Tibet. Acta Geologica Sinica, 88, 517-529.

Litasov, K.G., Kagi, H., and Bekker, T.B. (2018). Enigmatic super-reduced phases in corundum from natural rocks: Possible contamination from artificia abrasive materials or metallurgical slags. Lithos, 340, 181-190.

Litasov K.G., Kagi, H., Voropaev, S.A., Hirata, T., Ohfuji, H., and Ishibashi, H. (2019). Comparison of enigmatic diamonds from the Tolbachik arc volcano (Kamchatka) and Tibetan ophiolites: Assessing the role of contamination by synthetic materials. Gondwana Research, 75, 16-27.

Matveev, S., Ballhaus, C., Fricke, K., Truckenbrodt, J., and Ziegenbein, D. (1997) Volatiles in the Earth's mantle: I. Synthesis of CHO fluids at 1273K and 2.4 GPa. Geochimica et Cosmochimica Acta, 61, 3081-3088.

Miyashiro, A. (1973) The Troodos ophiolite complex was probably formed in an island arc. Earth and Planetary Science Letters, 19, 218-224.

Muan, A., and Somiya, S. (1959) Phase equilibrium studies in the system iron oxide-$Al_2O_3$-$Cr_2O_3$. Journal of the American Ceramic Society, 42, 603-613.

Münker, C., Pfänder, J.A., Weyer, S., Büchl, A., Kleine, T., and Mezger, K. (2003) Evolution of planetary cores and the Earth-Moon system from Nb/Ta systematics. Science, 301, 84-87.

Murray, J. L. (1989). Al-V (aluminum-vanadium). Bulletin of Alloy Phase Diagrams, 10, 351–357. doi:10.1007/bf02877591.

Nicholas, A. (1999) Les Montagnes sous la Mer. Editions du B.R.G.M., Orléans.

O'Neill, H.St.C. (1987) The quartz-fayalite-iron and quartz-fayalite-magnetite equilibria and the free energies of formation of fayalite ($Fe_2SiO_4$) and magnetite ($Fe_3O_4$). American Mineralogist, 72, 67-75.

O'Neill, H.St.C., and Wall, V.J. (1987) The olivine-orthopyroxene-spinel oxygen geobarometer, the nickel precipitation curve, and the oxygen fugacity of the Earth's Upper Mantle. Journal of Petrology, 28, 1169-1191.

O'Neill, H.St.C., Pownceby, M.I., and McCammon, C.A. (2003) The magnesiowüstite - iron equilibrium and its implications for the activity-composition relations of $(Mg,Fe)_2SiO_4$ olivine solid solutions. Contributions to Mineralogy and Petrology, 146, 308–325.

O'Neill, H.St.C., and Palme, H. (2014) Cosmochemical estimates of mantle composition. In: Treatise on Geochemistry 2nd Edition
http://dx.doi.org/10.1016/B978-0-08-095975-7.00201-1

Pearce, J.A., and Robinson, P.T. (2010) The Troodos ophiolitic complex probably formed in a subduction initiation, slab edge setting. Gondwana Research, 18, 60–81.

Pujol-Solà, N., Garcia-Casco, A., Proenza, J.A., González-Jiménez, J.M., del Campo, A., Colás, V., Canals, A., Sánchez-Navas A., and Roqué-Rossell, J. (2020) Diamond forms during low-pressure serpentinization of oceanic lithosphere. Geochemical Perspectives Letters, in press.

Putnis, A. (2002) Mineral replacement reactions: from macroscopic observations to microscopic mechanisms. Mineralogical Magazine, 66, 689–708.

Robertson, A.H.F. (2002) Overview of the genesis and emplacement of Mesozoic ophiolites in the Eastern Mediterranean Tethyan region. Lithos, 65, 1-67.

Robinson, P.T., Bai, W.J., Malpas, J., Yang, J.-S., Zhou, M.-F., Fang, Q.-S., Hu, X.-F., Cameron, S., and Staudigel, H. (2004) Ultra-high pressure minerals in the Luobusa Ophiolite, Tibet, and their tectonic implications. Geological Society of London, Special Publication, 226, 247–271.

Rohrbach, A., Ballhaus, C., Golla-Schindler, U., Ulmer, P., Kamenetsky, V.S., and Kuzmin, D.V. (2007) Metal saturation in the upper mantle. Nature 449, 456-458.

Schmidt, M.W., Gao, C., Golubkova, A., Rohrbach, A., and Connolly, J.A.D. (2014) Natural moissanite (SiC) - a low temperature mineral formed from highly fractionated ultra-reducing COH-fluids. Progress in Earth and Planetary Science, 1, 27. doi.org/10.1186/s40645-014-0027-0

Schreiber, H.D. (1979) Experimental studies of nickel and chromium partitioning into olivine from synthetic basaltic melts. 10th Lunar and Planetary Science Conference 509-516.

Shiryaev, A.A., and Gaillard, F. (2014). Local redox buffering by carbon at low pressures and the formation of moissanite–natural SiC. European Journal of Mineralogy, 26, 53-59.

Stubican, V.S., and Greskovich, C. (1975) Trivalent and divalent chromium ions in spinel. Geochimica et Cosmochimica Acta, 39, 875-881.

Sung, C.-M., and Tai, M.-F. (1997) Reactivities of transition metals with carbon: Implications to the mechanism of diamond synthesis under high pressure. International Journal of Refractory Metals and Hard Materials, 15, 237–256.

Sutton, S.R., Jones, K.W., Gordon, B., Rivers, M.L., Bajt, S., and Smith, J.V. (1993) Reduced chromium in olivine grains from lunar basalt 15555: X-ray Absorption Near Edge Structure (XANES). Geochimica et Cosmochimica Acta, 57, 461-468.

Tan, X. (2014) Catalyst alloys processing. JOM 66, 2176–2185. doi.org/10.1007/s11837-014-0984-1

Taylor, W.R., and Green, D.H. (1989) The role of reduced C-H-O fluids in mantle partial melting. In: Kimberlites and Related Rocks: Their Composition, Occurrence, Origin and Emplacement (Ross J., Editor). Geological Society of Australia, Special Publication, 14, 592-602.

Ulmer, G.C., Grandstaff, D.E., Woermann, E., Göbbels, M., Schönitz, M., and Woodland, A.B. (1998) The redox stability of moissanite (SiC) compared with metal-metal oxide buffers at 1773 K and at pressures up to 90 kbar. Neues Jahrbuch für Mineralogie Abhandlungen, 172, 279 - 307

Wade, J., and Wood, B. (2001) The Earth's ‘missing ’niobium may be in the core. Nature, 409, 75–78 (2001). https://doi.org/10.1038/35051064

Wirth, R. (2009) Focused Ion Beam (FIB) combined with SEM and TEM: advanced analytical tools for studies of chemical composition, micro-structure and crystal structure in geomaterials on a nanometer scale. Chemical Geology, 261, 217–229.

Wiser, N.M., and Wood, B.J. (1991) Experimental determination of activities in Fe−Mg olivine at 1400 K. Contributions to Mineralogy and Petrology, 108, 146–153.

Witt-Eickschen, G., and O'Neill, H.St.C (2005) The effect of temperature on the equilibrium distribution of trace elements between clinopyroxene, orthopyroxene, olivine and spinel in upper mantle peridotite. Chemical Geology, 221, 65-101.

Xiong, F., Yang, J., Robinson, P.T., Xu, X., Liu, Z., Li, Y., Li, J., and Chen, S. (2015) Origin of podiform chromitite, a new model based on the Luobusa ophiolite, Tibet. Gondwana Research, 27, 525-542.

Xiong, Q., Griffin, W.L., Huang, J.-X., Gain, S.E.M., Toledo, V., Pearson, N.J., and O'Reilly, S.Y. (2017) Super-reduced mineral assemblages in “ophiolitic” chromitites and peridotites: the view from Mount Carmel. European Journal of Mineralogy DOI: 10.1127/ejm/2017/0029-2646.

Xiong, F., Liu, Z., Kapsiotis, A., Yang, J., Lenaz, D., and Robinson, P.T. (2019) Petrogenesis of lherzolites from the Purang ophiolite, Yarlung-Zangbo suture zone, Tibet: origin and significance of ultra-high pressure and other ‘unusual ’minerals in the Neo-Tethyan lithospheric mantle. International Geological Review, https://doi.org/10.1080/00206814.2019.1584771.

Xu, X., Yang, J., Robinson, P.T., Xiong F., Ba, D., and Guo, G. (2015) Origin of ultrahigh pressure and highly reduced minerals in podiform chromitites and

associated mantle peridotites of the Luobusa ophiolite, Tibet. Gondwana Research, 27, 686–700.

Xu, X., Cartigny, P., Yang J., Dilek Y., Xiong F., and Guo, G. (2017) Fourier transform infrared spectroscopy data and carbon isotope characteristics of the ophiolite-hosted diamonds from the Luobusa ophiolite, Tibet, and Ray-Iz ophiolite, Polar Urals. Lithosphere, 10, 156–169.

Yang, J., Dobrzhinetskaya, l.F., Bai, W.J., Junfeng Zhang, J., and Green II, H.W. (2007) Diamond and coesite-bearing chromitites from the Luobusa ophiolite, Tibet. Geology, 35, 875–878.

Yang, J., Robinson, P.T., and Dilek, Y. (2014) Diamonds in ophiolites: A little-known diamond occurrence. Elements, 10, 127–130.

Yang, J., Meng, A., Xu, X., Robinson, P.T., Dilek, Y., Makeyev, A.B., Wirth, R., Wiedenbeck, M., Griffin, W.L., and Cliff, J. (2015) Diamonds, native elements and metal alloys from chromitites of the Ray-Iz ophiolite of the Polar Urals. Gondwana Research, 27, 459–485.

Yang, J.S., Trumbull, R.P., Robinson, P.T., Xiong, F.H., and Lian, D.Y. (2018) Comment 2 on “Ultra-high pressure and ultra-reduced minerals in ophiolites may form by lightning strikes”. Geochemical Perspectives Letters, 8, 6-7.

Zhou, L., Jia, X.-P., Ma, H.A., Zheng, Y.-J., and Li, Y.-T. (2009) Industrial diamonds grown in $Ni_{70}Mn_{25}Co_5$–graphite–sulfur system under HPHT. Chinese Physics, B18, 333-338.

Zuxiang, Y. (1984) Two new minerals gupeiite and xifengite in cosmic dusts from Yanshan. Acta Petrologica Mineralogica et Analytica, 3 (abstract).

748 Figure Captions

749 Figure 1. Textures of ultra-reduced minerals in ophiolites and Kishon River
750 aggregates.

751 A - an Fe-Si-Ti-P symplectite from Luobusa documented by Robinson et al.
752 (2004). Tubular inclusions enriched in metallic Ti and P but essentially Fe-Si
753 alloys. Texturally it seems they exsolved from the Fe-Si matrix and were preserved
754 *in-situ* because of rapid quenching.

755 B and C - details of a zonar Fe-Ti-Si grain aggregate recovered from a bulk
756 chromite sample from Luobusa (Yang et al., 2007; Dobrzhinetskaya et al. 2009). In
757 the original Figure (Yang et al., 2007) the Fe-Ti symplectites are surrounded by
758 rims of Fe-Ti alloy, native Ti, pseudomorphs of coesite after stishovite, and
759 kyanite. Dobrzhinetskaya et al. (2009) documented within coesite of this aggregate
760 nanoscale Ti nitrides.

761 D - an Ni-(Fe-Cr)-C carbide grain with skeletal Cr carbide needles, recovered from
762 concentrates of a 500 kg chromitite bulk sample from Luobusa (Robinson et al.,
763 2004).

764 E and F - V-Al, TiN, and $Ti_2O_3$ skeletons with metallic V and a vanadium hydride
765 ($VH_2$) grain attached, in corundum (co) matrix (Griffin et al., 2016b; 2019; Bindi et
766 al., 2019). For discussion of these fragments see text.

767 G - a BSE image of "*in-situ*" SiC fragments in chromite from Luobusa (Liang et
768 al., 2014), claimed to be lower mantle derived. The dark (low atomic number
769 contrast) matrix around the SiC fragments is not specified, potentially a void or
770 carbon. Note that the host chromite is not stable at pressures prevalent in the ower
771 mantle (Chen et al., 2003).

H and I - aggregates of euhedral "qusongite" (WC) grains in a Co metal matrix (Fang et al., 2009; Yang et al. 2015). The two photos are identical (cf. one WC grain outlined in red for orientation) although they supposedly come from different WC aggregates of two different ophiolites (Ray Iz and Luobusa) 4600 km apart (see text).

J - skeletal ferroan ringwoodite (Rw), now ahrensite, in a glassy pumice from Spain (Díaz-Martinez and Ormö, 2003). Although ringwoodite is not an ultra-reduced mineral this photo is included in the compilation of disequilibrium morphologies to illustrate that UHP phases need not be UHP but can grow metastable at much lower pressures than their equilibrium pressures.

All images modified from the original sources to avoid copyright conflicts.

Figure 2. Oxygen fugacities imposed by the assemblages fayalite-magnetite-quartz (FMQ), iron-wüstite (IW), $Ti_2O_3$-$TiO_2$, and SiC-$SiO_2$-C. The FMQ and IW buffers are from O'Neill (1987), the other equilibria were calculated using thermodynamic data by Barin (1995). The dashed line approximates experimental $fO_2$ conditions as described in the text. All calculations for 1 atm. Redox gradient at 1600K marked by arrows. Higher pressure changes absolute fugacities but the $fO_2$ differences among the buffers and the 1/T - ($\Delta$H / RT) slopes remain largely unaffected by pressure.

Figure 3. Backscattered images of the experimental runs. A - BSE image illustrating reduction rims around two olivine ($Fo_{89}$) relicts that reacted with SiC (cr-6); positions of three FIB foils marked in red. B - reduced olivine with exsolved Fe-Ni metal, in C and D element maps of Ni and Mg; most magnesian olivine

marked by arrows. E and F - relict Bushveld chromite surrounded by reduced spinel slightly lower in atomic number contrast; bright veinlets are (Fe,Cr) metal. G - zoned Al-spinel surrounded by silicate melt (now glass). H - spinel aggregate with chromite cores veined by (Fe,Cr) metal; one FIB foil marked in red, white frame mapped for element distribution (Fig. 4). I - SiC grain with $SiO_2$ reaction rim. J - $SiO_2$ reaction rim around SiC in high resolution. K - Fe-Cr±Si±C metal grain (former melt?) exsolved to Cr, Si, and Fe enriched fractions; red frame mapped for element distributions.

Figure 4. Element maps of the chromite aggregate of Figure 3H illustrating compositional effects upon reduction by SiC. Warmer colors indicate higher concentrations. For position see frame in Fig. 3H.

Figure 5. TEM images of run products. A - forsterite (~ $Fo_{96}$) with Fe-Ni metal inclusions in reduction rim around relict olivine (cf. Fig. 3A); the Fast Fourier Transform (FFT) as inset to illustrate that the metal inclusions are cubic α-(Fe,Ni). B - reduced spinel with cubic (Fe,Cr)° metal and cubic ferroan periclase inclusions marked in red (FFT as inset). C - euhedral (Fe,Cr)° metal grains in reduced spinel. D - bright field image of defect-rich spinel, FFT to illustrate that the spinels are cubic; the dark schlieren are dislocations.

Figure 6. Chromite compositions (atomic ratios). Black symbols illustrate oxidised LG-1 Bushveld chromites (~ FMQ) plus their relicts, blues symbols secondary spinel compositions that formed by reaction with SiC, red symbols reduced spinels that reacted with silicate melt.

Figure 7. The reduced side of the C-H-O phase diagram. Grey circles denote graphite-saturated C-H-O fluid compositions synthesised by Matveev et al. (1997) at 1273K and 2.4 GPa. Species of fluids along the C saturation line are $CH_4$, $H_2O$, $H_2$, and minor $C_2H_6$. Molar H-O ratios are indicated by contours. Oxygen buffer assemblages (red dots) along the C saturation line are SiC-$SiO_2$-C (SiC, H/O ~ 1000), Fe-FeO (IW, H/O ~ 30), WC-$WO_2$-C (WCO, H/O ~ 14), and Co-CoO (CoO, H/O ~ 4.3). Increasing temperature increases C solubility and shifts the $H_2O$ maximum (inset) to higher C content (Taylor and Green, 1989). Increasing pressure has the opposite effect.

Figure 8. Pressure-volume relations of a $CH_4$-$H_2$ (94/6) fluid in redox equilibrium with SiC at 1600K, calculated with an MRK equation of state (Anderson and Crerar, 1993).

This is the peer-reviewed, final accepted version for American Mineralogist, published by the Mineralogical Society of America.
The published version is subject to change. Cite as Authors (Year) Title. American Mineralogist, in press.
DOI: https://doi.org/10.2138/am-2021-7612. http://www.minsocam.org/


Table 1. Starting materials and experimental phase compositions of three experimental runs at 1600K and 0.7 GPa, with run times ranging from 30 min (cr-9), 2 hrs (cr-6), and 4 hrs (cr-8). $Fe_2O_3$ and CrO where listed were calculated assuming stoichiometry. Cr# = atomic Cr/(Cr + Al + $Fe^{3+}$), Mg# = atomic Mg/(Mg + $Fe^{2+}$), - not detected, n.c. not calculated.

| | Starting materials | | | Experimental compositions, 1600K, 0.7 GPa | | | | | | | |
|---|---|---|---|---|---|---|---|---|---|---|---|
| | oxidised | | | reduced | | | | | | | |
| | olivine | opx | chromite | olivine | olivine | olivine | opx | spinel | spinel | spinel | spinel |
| Oxide | 1 | 2 | 3 | 4 | 5 | 6 | 7 | 8 | 9 | 10 | 11 |
| $SiO_2$ | 40.9 | 55.7 | 0.14 | 41.7 | 42.1 | 42.3 | 52.6 | - | - | 0.14 | 0.11 |
| $TiO_2$ | - | 0.12 | 0.59 | 0.04 | 0.01 | 0.03 | 0.37 | 0.50 | 0.74 | 0.21 | 0.27 |
| $Al_2O_3$ | 0.05 | 1.60 | 15.4 | 0.2 | 0.09 | 0.09 | 4.2 | 14.5 | 17.2 | 53.5 | 56.6 |
| $Cr_2O_3$ | 0.2 | 0.8 | 47.7 | - | - | - | - | 59.8 | 51.5 | 12.1 | 13.5 |
| $Fe_2O_3$ | - | - | 6.20 | - | - | - | - | n.c. | n.c. | n.c. | n.c. |
| CrO | - | - | - | 1.8 | 3.5 | 3.6 | 2.2 | n.c. | n.c. | n.c. | n.c. |
| FeO | 10.7 | 6.1 | 16.6 | 3.03 | 2.49 | 2.4 | 2.47 | 3.20 | 8.10 | 11.8 | 6.12 |
| NiO | 0.3 | n.a. | n.a. | - | - | - | - | - | - | - | - |
| MgO | 48.2 | 32.2 | 11.8 | 53.5 | 52.4 | 52.5 | 35.4 | 20.2 | 22 | 21 | 22.7 |
| CaO | 0.15 | 2.64 | - | 0.23 | 0.19 | 0.19 | 2.16 | - | - | - | - |
| Total | 100.5 | 99.2 | 98.4 | 100.4 | 100.9 | 101.1 | 99.4 | 98.2 | 99.8 | 98.8 | 99.2 |
| cations | 3.00 | 4.00 | 3.00 | 3.00 | 3.00 | 2.99 | 4.00 | 3.00 | 3.06 | 3.03 | 3.00 |
| Mg# | 0.89 | 0.90 | 0.56 | 0.97 | 0.97 | 0.98 | 0.96 | 0.92 | 0.83 | 0.76 | 0.87 |
| Cr# | - | - | 0.62 | - | - | - | - | 0.74 | 0.67 | 0.13 | 0.14 |
| relat. $fO_2$ | --------- FMQ ------- | | | ---------- ~ IW-3 ---------- | | | | | | | |

This is the peer-reviewed, final accepted version for American Mineralogist, published by the Mineralogical Society of America.
The published version is subject to change. Cite as Authors (Year) Title. American Mineralogist, in press.
DOI: https://doi.org/10.2138/am-2021-7612. http://www.minsocam.org/

# Fig. 1

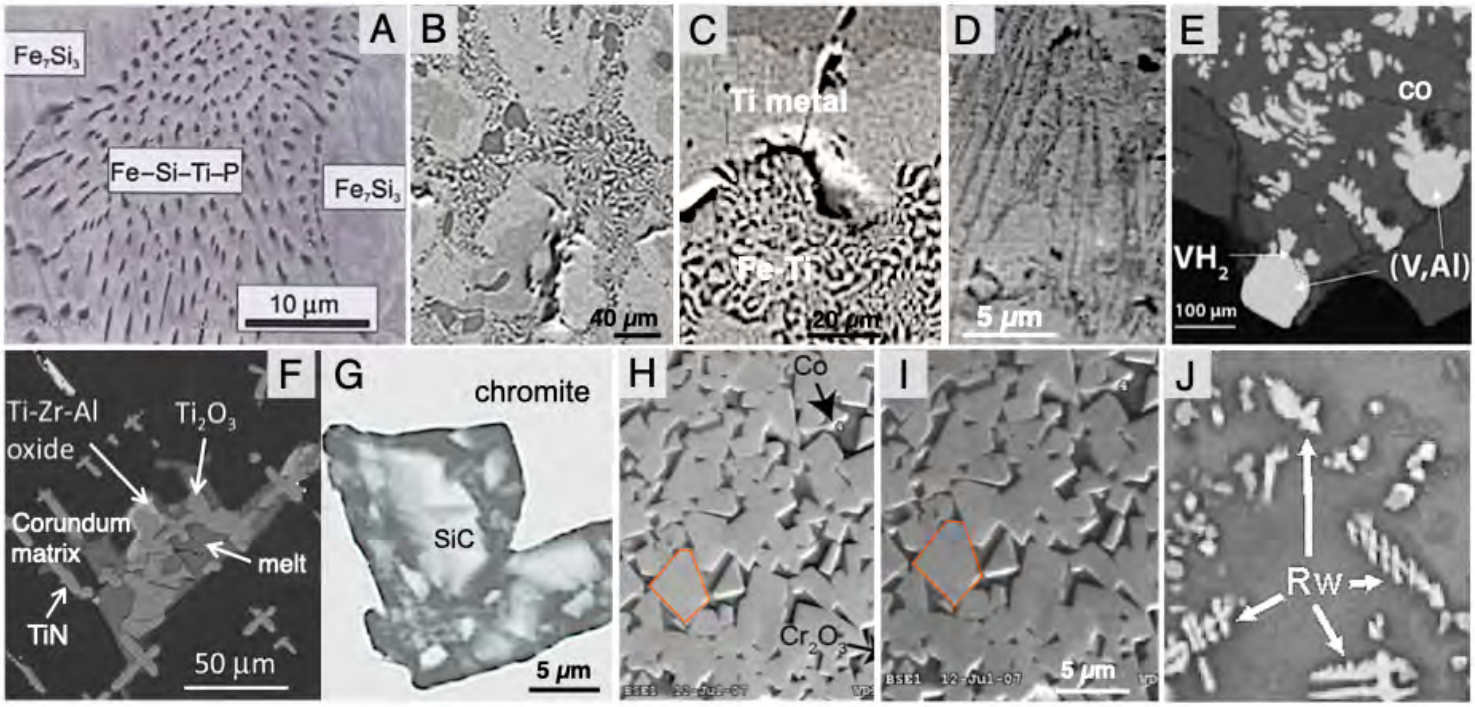

Fig. 2

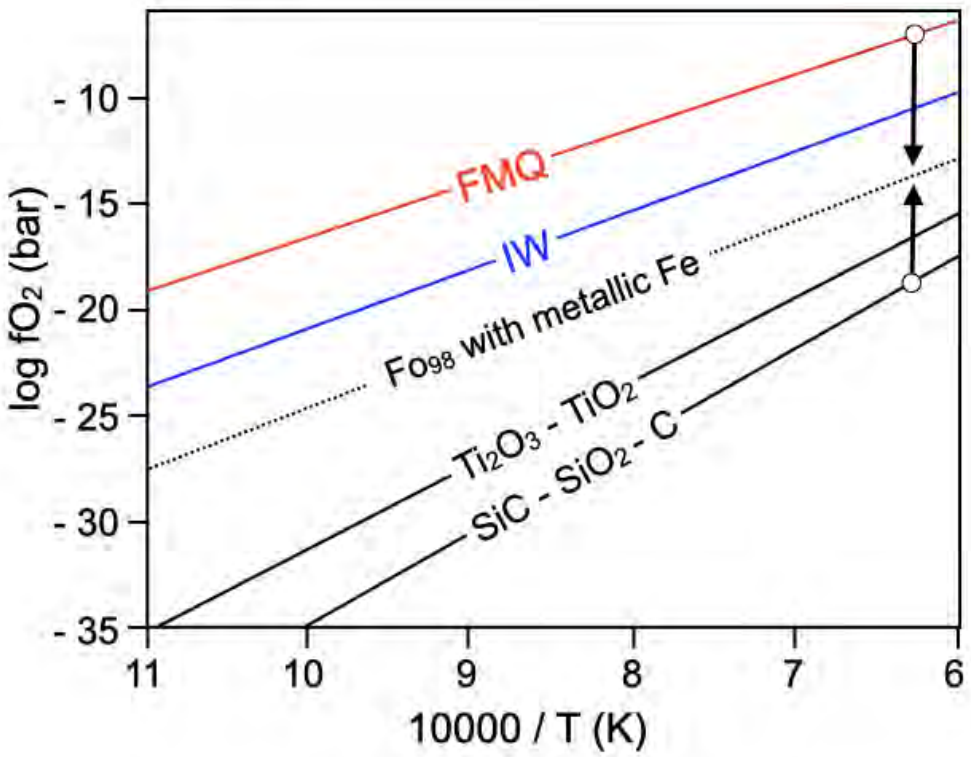

This is the peer-reviewed, final accepted version for American Mineralogist, published by the Mineralogical Society of America.
The published version is subject to change. Cite as Authors (Year) Title. American Mineralogist, in press.
DOI: https://doi.org/10.2138/am-2021-7612. http://www.minsocam.org/

Fig. 3

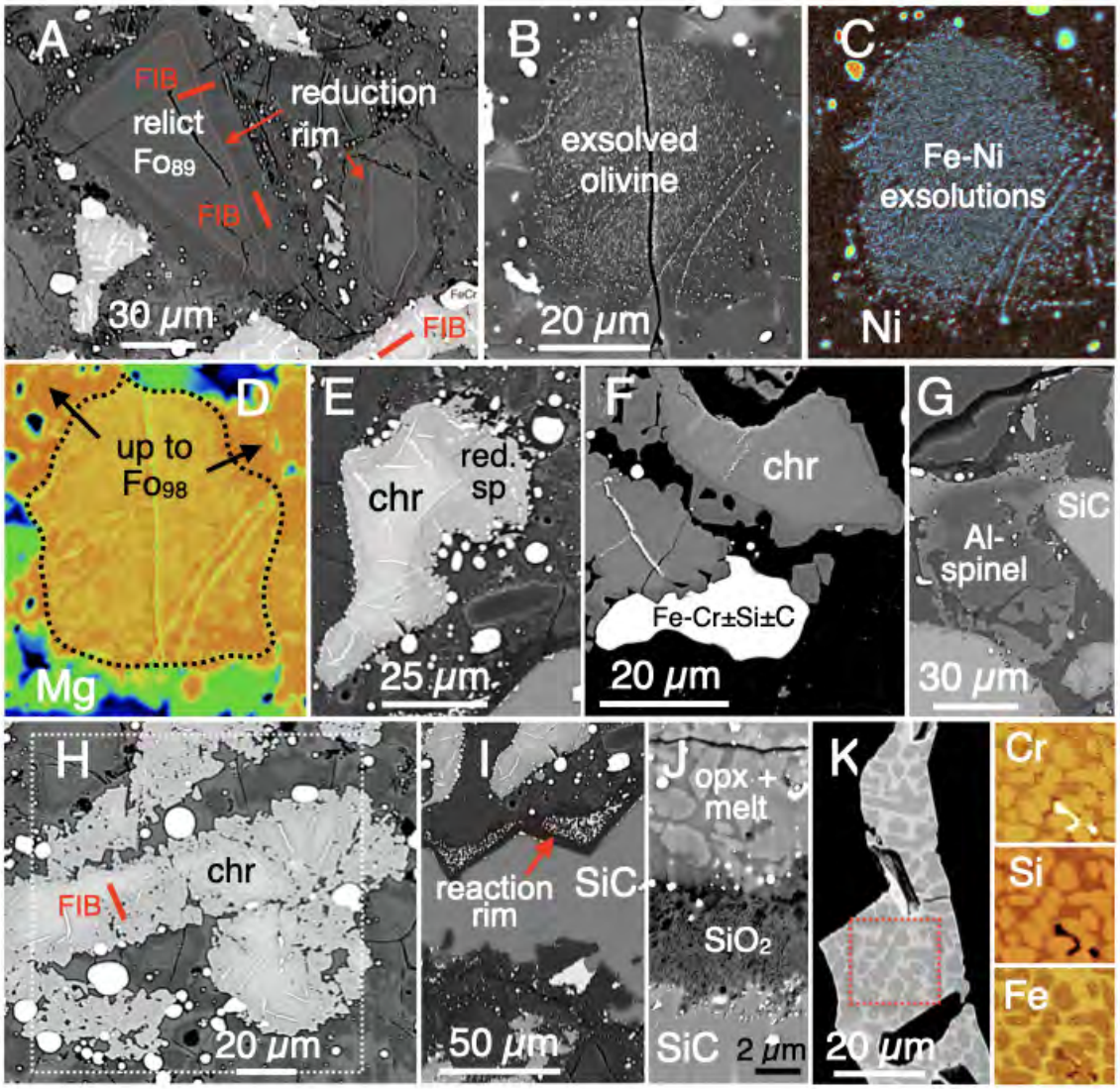

This is the peer-reviewed, final accepted version for American Mineralogist, published by the Mineralogical Society of America.
The published version is subject to change. Cite as Authors (Year) Title. American Mineralogist, in press.
DOI: https://doi.org/10.2138/am-2021-7612. http://www.minsocam.org/

Fig. 4

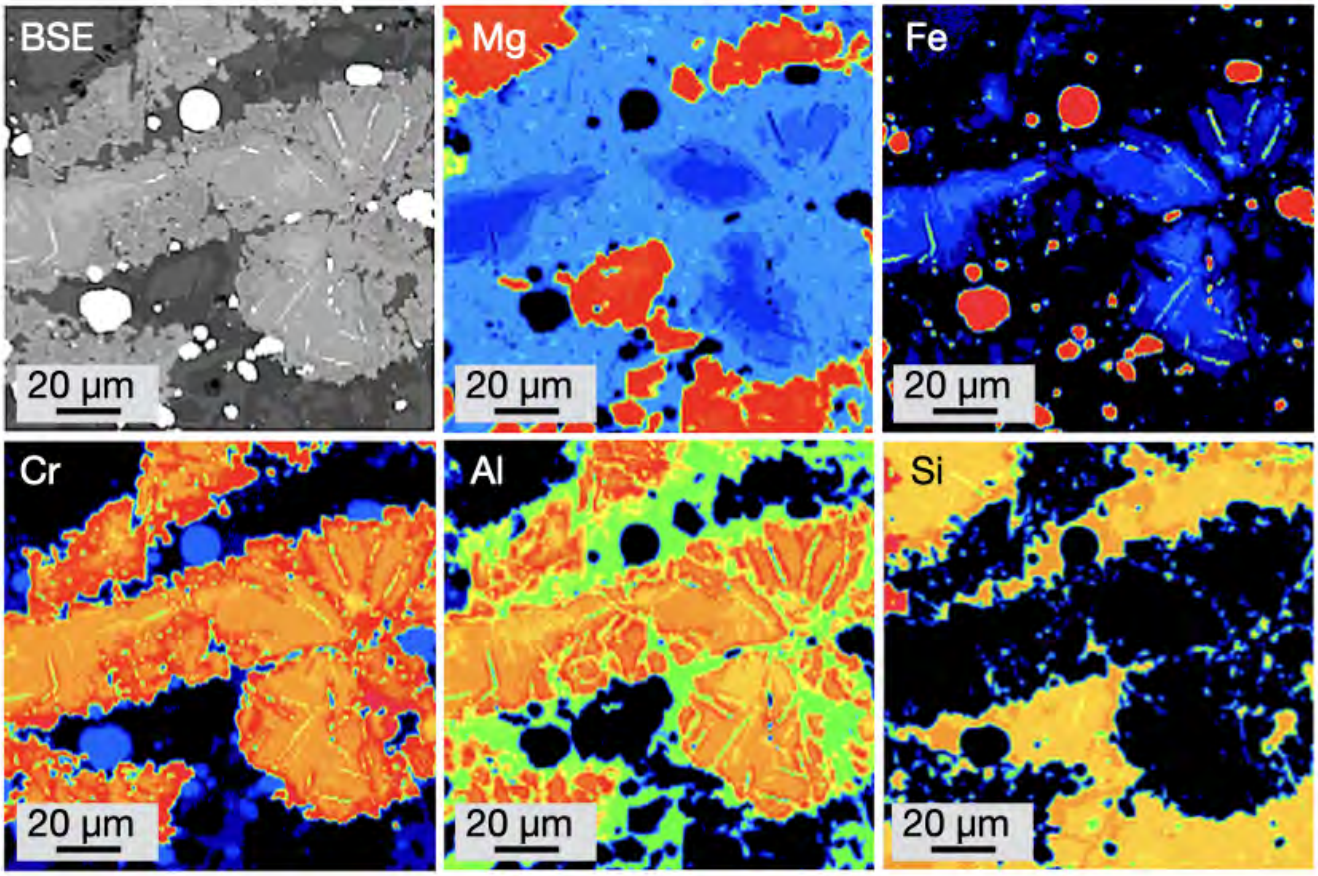

This is the peer-reviewed, final accepted version for American Mineralogist, published by the Mineralogical Society of America.
The published version is subject to change. Cite as Authors (Year) Title. American Mineralogist, in press.
DOI: https://doi.org/10.2138/am-2021-7612. http://www.minsocam.org/

Fig. 5

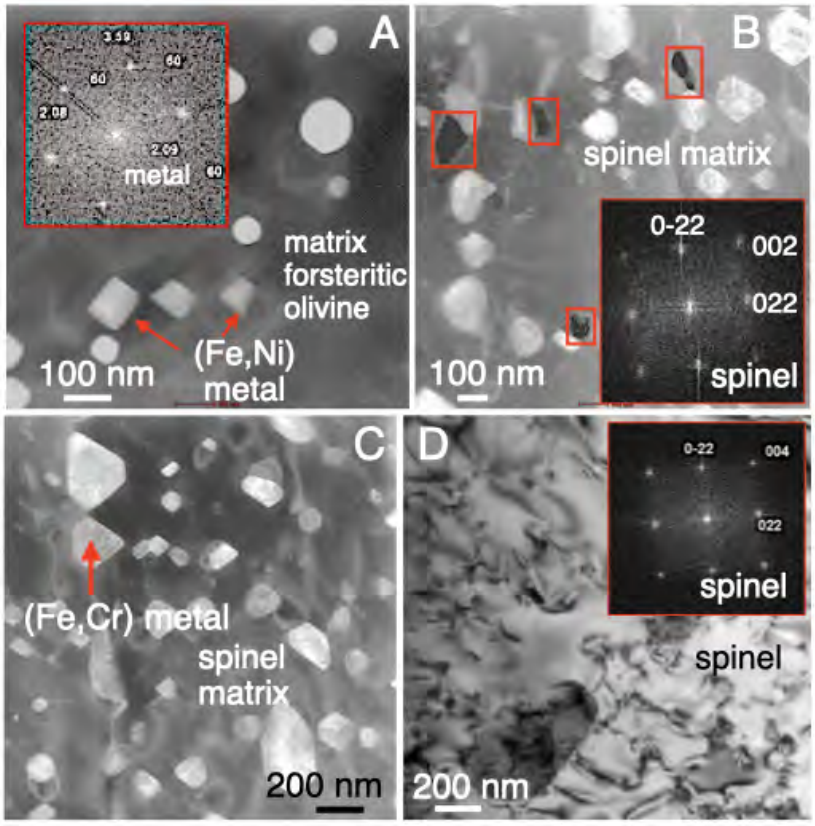

This is the peer-reviewed, final accepted version for American Mineralogist, published by the Mineralogical Society of America.
The published version is subject to change. Cite as Authors (Year) Title. American Mineralogist, in press.
DOI: https://doi.org/10.2138/am-2021-7612. http://www.minsocam.org/

Fig. 6

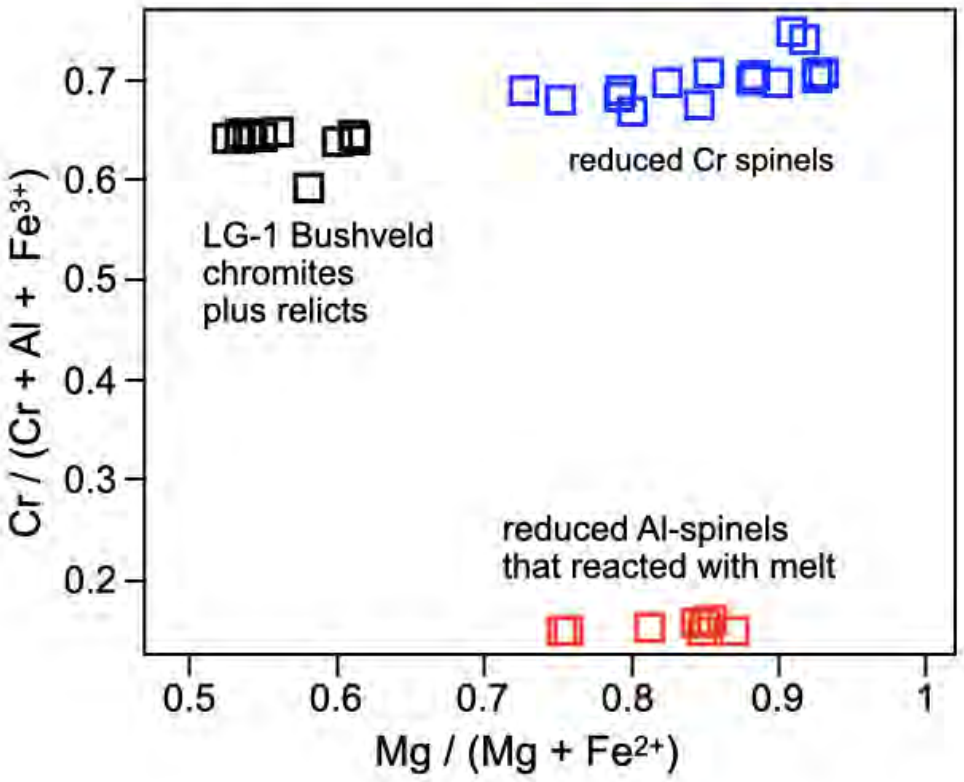

This is the peer-reviewed, final accepted version for American Mineralogist, published by the Mineralogical Society of America.
The published version is subject to change. Cite as Authors (Year) Title. American Mineralogist, in press.
DOI: https://doi.org/10.2138/am-2021-7612. http://www.minsocam.org/

Fig. 7

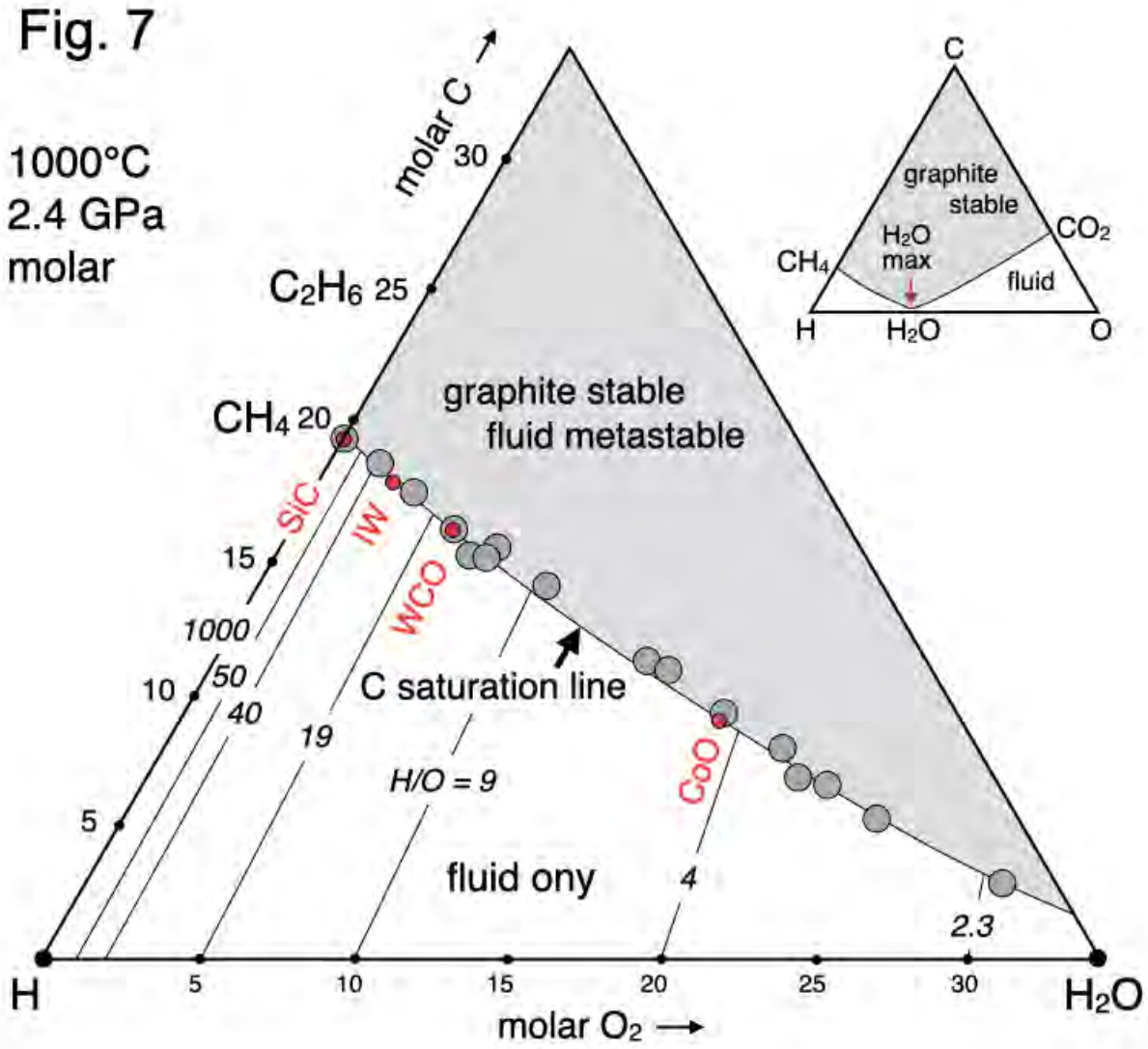

Fig. 8